

000 001 002 003 004 005 CAUSAL3D: A COMPREHENSIVE BENCHMARK FOR 006 CAUSAL LEARNING FROM VISUAL DATA 007 008 009

010 **Anonymous authors**
011
012
013
014
015
016
017
018
019
020
021
022
023
024
025
026
027
028
029
030
031
032
033
034
035
036
037
038
039
040
041
042
043
044
045
046
047
048
049
050
051
052
053

Paper under double-blind review

ABSTRACT

True intelligence hinges on the ability to uncover and leverage hidden causal relations. Despite significant progress in AI and computer vision (CV), there remains a lack of benchmarks for assessing models’ abilities to infer latent causality from complex visual data. In this paper, we introduce **CAUSAL3D**, a novel and comprehensive benchmark that integrates structured data (tables) with corresponding visual representations (images) to evaluate causal reasoning. Designed within a systematic framework, Causal3D comprises 19 3D-scene datasets capturing diverse causal relations, views, and backgrounds, enabling evaluations across scenes of varying complexity. We assess multiple state-of-the-art methods, including classical causal discovery, causal representation learning, and large/vision-language models (LLMs/VLMs). Our experiments show that as causal structures grow more complex without prior knowledge, performance declines significantly, highlighting the challenges even advanced methods face in complex causal scenarios. Causal3D serves as a vital resource for advancing causal reasoning in CV and fostering trustworthy AI in critical domains.

1 INTRODUCTION

Computer vision (CV) has achieved remarkable success in tasks such as classification (Dosovitskiy et al., 2021; Singh et al., 2022; Fang et al., 2023) and detection (Liu et al., 2021; Wang et al., 2023). Although these systems excel at identifying statistical correlations within data, they often struggle to infer deeper causal relations. This limitation significantly impacts their ability to be applied to high-stakes domains or unseen scenes. For instance, without understanding the causal relations between object depths, motions, and shapes, a vision-based autonomous driving system may easily misidentify traffic signs due to spurious correlations or adversarial attacks, leading to sudden braking and severe safety issues (Yang et al., 2022).

Unlike classification and detection tasks, which have thrived on large-scale datasets with explicit labels, causal tasks in images demand more for study and evaluation — ideally, annotations with clear causal relations among variables. This makes dataset collection significantly more challenging than in traditional CV tasks. The difficulty stems from two key factors: **inherent complexity and covert nature of causality**: Real-world causal relations are often complex and not directly observable, and causal variables are often high-level concepts (e.g., an object) instead of low-level pixels, making causal relations in vision domain inherently challenging to discern; **challenges in visual representation**: Even well-established causal rules are challenging to visually depict. For example, in physics, magnetic fields are represented by invisible magnetic induction lines, making them difficult to illustrate in realistic images. Similarly, abstract concepts like economic principles, (e.g., supply and demand), are not easily encoded into visual forms.

Some existing datasets have been involved in causal studies in visual AI systems. However, these datasets often have significant limitations. For instance, oversimplified 2D hypothetical datasets (Yang et al., 2020) fail to capture the richness and complexity of real-world environments. Similarly, domain-specific datasets like the CelebA face dataset (Liu et al., 2015) are not designed for causal reasoning and lack the structural diversity required for comprehensive explorations. Recent datasets developed for vision- and multimodal-language models (VLMs/MLMs) (Zimmermann et al., 2021; Von Kügelgen et al., 2021; Mao et al., 2022; Tung et al., 2024) have improved in complexity and realism but remain limited in explicitly representing causality and in offering diverse

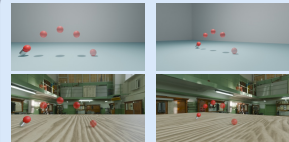
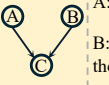
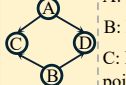
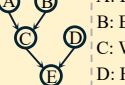
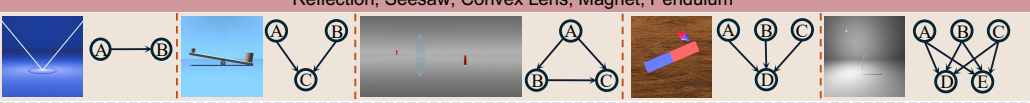
054	 Multi-View Images  Descriptions  Causal Graph  Structure Equations	Spring 	Parabola 	Water Flow 
055		<i>A wooden cube is on a spring.</i>	<i>A ball is launched by a compressed spring, forming a parabolic trajectory.</i>	<i>A ball is in a beaker filled with water. A hole on the side of the beaker shoots water out.</i>
056		 A: Weight of the cube. B: Stiffness coefficient of the spring. C: Spring's deformation.	 A: Spring's deformation. B: Launch angle. C: Height of the highest point. D: Horizontal distance.	 A: Ball's volume. B: Beaker bottom's radius. C: Water's height. D: Hole's height. E: Horizontal distance of the water flow.
057	$C = \frac{A}{B}$		$C = kA^2 \sin^2(B)/2mg$ $D = kA^2 \sin(2B)/mg$	$C = h_0 + 4A/\pi B^2$ $E = 2\sqrt{D(C-D)}$
058	Reflection, Seesaw, Convex Lens, Magnet, Pendulum 			
059				
060				
061				
062				
063				
064				
065				
066				
067				
068				
069				
070				
071				
072				
073				
074				
075				

Figure 1: The proposed **CAUSAL3D** dataset. We display 8 real-world scenes (11 hypothetical scenes are in the Appendix 6). We focus on 3 scenes: springs, parabolas, and water flow. 1) The blue block represents multi-view images of each scene, offering four different views. The first row shows virtual backgrounds, while the second row shows real backgrounds, with the same view in each column; 2) The green block provides textual descriptions; 3) The yellow block represents the causal graphs for each scene, along with the meanings of each variable in the graphs; 4) The pink block shows the structural equations (i.e., functions describing causal relations) for each scene. The bottom row briefly presents an overview of the remaining 5 real-world scenes and their corresponding causal graphs, including reflection, seesaw, convex lens, magnet, and pendulum. Detailed information on these 5 scenes can be found in the Appendix 6.

causal relations. The absence of clearly defined causal relations within visual representations, along with the lack of tabular records that are tightly aligned with these representations to provide guidance, makes such physics-aware VLMs/MLMs datasets suboptimal for fine-grained causal reasoning tasks. Especially, as interest in 3D data grows, causal learning in 3D settings introduces new challenges, opportunities, and insights. The complexity of realistic 3D scenes—encompassing lighting, texture, background, and viewpoint—can introduce spurious correlations and backdoor paths, making causal inference more difficult. At the same time, 3D environments provide multi-view consistency, allowing models to observe the same underlying causal relationships from diverse perspectives, which helps disentangle true causality from viewpoint-dependent features. This makes **3D datasets uniquely valuable for developing and evaluating robust, causally grounded models in realistic settings**. However, this area remains underexplored.

In general, existing visual datasets either lack explicit definitions of causal relations beyond visual representation or are too specific and simplified to enable comprehensive exploration of diverse causal relations. On the other hand, datasets in the causal research community, while rich in diverse causalities and clear causal definitions, lack corresponding visual representations, making them unsuitable for tasks involving causal reasoning in images, not to mention complicated 3D scenarios. This disconnect makes it challenging to effectively advance and evaluate AI systems’ abilities of reliable reasoning, thereby creating a significant bottleneck in advancing this field.

To address these limitations, we introduce **CAUSAL3D**, the first benchmark specifically designed to systematically explore and evaluate causality learning through a combination of realistic 3D imagery and explicit causal structures (i.e., causal graphs and structure equations). Using **CAUSAL3D**, we conduct experiments on existing algorithms and tools, **establishing a comprehensive benchmark** to evaluate models’ abilities to identify and leverage diverse causal relations.

108
 109
 110
 111
 112 Table 1: Qualitative comparison between Causal3D and other causality related dataset. “Diverse
 113 Structure” refers to whether the dataset covers different causal graph structures, e.g., our dataset
 114 involves 13 different graph structures spanning from real and hypothetical scenes.

Dataset	Dual Representation of Causality		Explicit Causal Structures		Hybrid Causal Framework		Diverse Structure and 3D Scenes	
	Tabular	Visual	Linear	Nonlinear	Physical Consistent	Hypothetical Scenes	Diverse Structure	Diverse 3D Scenes
CauseMe (Runge et al., 2019a)	✓	✗	✓	✓	✗	✓	✗	✗
CelebA (Liu et al., 2015)	✓	✓	✗	✗	✗	✓	✗	✗
CausalVAE (Yang et al., 2020)	✓	✗	✓	✓	✓	✓	✗	✗
Causal3DIdent (Zimmermann et al., 2021)	✗	✓	✓	✗	✓	✗	✗	✓
Craft (Ates et al., 2022)	✗	✗	✓	✗	✓	✗	✗	✗
CLEVR-Humans (Mao et al., 2022)	✗	✓	✓	✗	✓	✗	✗	✓
Physion++ (Tung et al., 2024)	✗	✓	✓	✓	✓	✗	✗	✓
Causal3D	✓	✓	✓	✓	✓	✓	✓	✓

120
 121 To the best of our knowledge, CAUSAL3D (see Fig. 1) is the first dataset tailored for causality studies
 122 that combines realistic 3D scenes with explicit causal graphs (i.e., Directed Acyclic Graphs (DAGs))
 123 representing variables as nodes and causal relations as edges). This dataset stands out due to several
 124 key features: **1) Dual Representation of Causality:** CAUSAL3D provides a dual representation of
 125 causality by including both tabular data (for high-level concepts) and strongly corresponding visual
 126 representations in multiple 3D scenes. This design provides sufficient information for causal studies
 127 in vision, enabling precise evaluations of models in related domains. **2) Diverse Design:** The
 128 difficulty in CAUSAL3D is diversely structured, derived from different dimensions, including the
 129 number of variables (ranging from 2 to 5), multiple causal structures, different (linear/nonlinear)
 130 types of causal relations, and various camera views and backgrounds in 3D scenes. This design
 131 enables benchmarking with progressively increasing levels of challenges, allowing for fine-grained
 132 evaluation of model performance. **3) Physically Consistent and Hypothetical Scenes:** CAUSAL3D
 133 encompasses both real-world and hypothetical scenes. By leveraging established physical rules, it
 134 creates datasets with realistic causal relations, enhancing the dataset’s authenticity. To further diversify
 135 causal scenes, CAUSAL3D incorporates hypothetical causal relations, providing a broader range
 136 of possibilities and enriching its utility for causality research. With the dataset, we designed systematic
 137 experiments to evaluate representative causal methods and LLMs/VLMs in different causal
 138 tasks. In this work, our primary contributions are threefold:

- **Dataset** We introduce CAUSAL3D, a novel and comprehensive benchmark consisting of 19 datasets that span a wide range of causal structures, viewpoints, and background variations within realistic 3D scenes. The full dataset will be released to support further research.
- **Evaluation** We implement a thorough evaluation of models on CAUSAL3D, spanning from traditional causal algorithms to advanced LLMs and VLMs for images, offering a detailed analysis of the current state-of-the-art models on our benchmark.
- **Insights** We lay a strong foundation for advancing causal learning in CV by bridging the gap between these fields through our benchmark and provide key insights from our experimental observations.

2 RELATED WORK

148
 149
 150 **Causal Discovery from Tabular Data** Causal discovery is an important task in causal inference
 151 (Pearl, 2009), aiming to identify the causal relations from data. Multiple methods have been developed
 152 for this task and most of them focus on tabular data (Wen et al., 2021; Tu et al., 2024; Wen
 153 et al., 2022; Cinquini et al., 2021; Russo and Toni, 2023). These methods mainly include constraint-
 154 based methods (e.g., PC (Spirtes et al., 2000b)) and score-based methods (e.g., GES (Chickering,
 155 2002)). Many of them are statistical methods (e.g., CAM (Bühlmann et al., 2014), LiNGAM (Yang
 156 et al., 2024)), which have good theoretical support but often suffer from strong assumptions, sensitivity,
 157 and scalability issues.

158 Recently, deep learning-based methods have attracted lots of attention due to their improvement in
 159 these aspects. Among them, causal-TGAN (Wen et al., 2022), GraN-DAG (Lachapelle et al., 2020),
 160 DAG-GNN (Yu et al., 2019)) can model nonlinear causal relations in large datasets. Diffusion-
 161 based approaches (e.g., DiffAN (Sanchez et al., 2023)) improve robustness against noises while
 being computationally intensive and sensitive to hyperparameters.

162 **LLM-based Causal Discovery** Recent advances in LLMs have broadened their role in causal dis-
 163covery (Ma, 2024; Jin et al., 2024; Liu et al., 2024b; Ban et al., 2023; Liu et al., 2024a; Wu et al.,
 164 2024; Wan et al., 2024; Shen et al., 2024). LLM-based causal discovery spans pairwise and full-
 165 graph discovery (Ma, 2024; Kıcıman et al., 2023; Jiralerpong et al., 2024), often leveraging prompts
 166 such as binary or multiple-choice selection and natural question-answering. Among them, many
 167 state-of-the-art models like ChatGPT 4o (Rawal et al., 2024) and Gemini-1.5 Pro (Carro et al., 2024)
 168 have been widely explored for causal inference. Besides, some causality-specific agents like Causal
 169 Copilot (Wang et al., 2024b) integrate LLMs for natural language-based causal queries. Despite
 170 its promising performance, LLMs still face key limitations, including difficulty in handling latent
 171 confounders and complex causal tasks.

172 **Causal Methods in CV** Causal inference in CV is essential for improving generalization and inter-
 173prettability (Yang et al., 2021; Schölkopf, 2022). Many causal tasks have thus been widely explored
 174 in image data, one of them is causal representation learning, which aims to uncover disentangled
 175 and causally meaningful representations corresponding to high-level variables from data (Liu et al.,
 176 2022; Deng et al., 2022; Schölkopf et al., 2021). Many representative approaches in this area are
 177 based on generative models (e.g., CausalVAE (Yang et al., 2023), DEAR (Shen et al., 2022)). How-
 178 ever, they often depend on strong assumptions (e.g., available annotation of high-level concepts) that
 179 may not always hold. Recently, explorations of VLMs in causal tasks under more general scenes
 180 have also attracted increasing attention (Wang et al., 2024a; Zhao et al., 2024).

181 **Causal Datasets in CV** Tabular data has long dominated causal inference research (Runge et al.,
 182 2019a; Runge, 2018; Runge et al., 2019b; Spirtes et al., 2000a; Zheng et al., 2018). With the recent
 183 increasing need for causal studies in different data types and modalities, the community in CV and
 184 VLM has also placed more emphasis on causality. Recent years have witnessed the emergence of
 185 image and video datasets for causal reasoning (Zimmermann et al., 2021; Ates et al., 2022; Mao
 186 et al., 2022; Tung et al., 2024), bridging the gap between CV learning and causal reasoning. Despite
 187 these datasets addressing the absence of visual data encoded with causality, most of them still remain
 188 limited. They either focus on specific scenes, restricting the diversity of causal relations or lack
 189 rigorous causal definitions—such as explicit causal graphs and structured tabular records—to cap-
 190 ture interactions among in-image variables. Consequently, a gap remains between traditional causal
 191 research and the study of causality in CV and VLM, as summarized in Tab. 1. This highlights the
 192 need for datasets that integrate explicit causal structures with both visual and tabular representations.

3 CAUSAL3D: THE PROPOSED BENCHMARK

195 We introduce CAUSAL3D, a realistic 3D image dataset designed for causal learning from *observa-*
 196 *tional* visual data. Aiming to bridge the gap between causal study and CV/VLM community,
 197 CAUSAL3D is established with structured tabular data and tightly aligned visual representation. To
 198 build a comprehensive benchmark for evaluating models’ ability to uncover causality, CAUSAL3D
 199 contains visual representations encoded with diverse causal relations among multiple variables. The
 200 dataset comprises two main components: **Physically Consistent 3D Scenes**, which simulate real-
 201 world settings to enhance the authenticity of the dataset, and **Hypothetical 3D Scenes**, introduced
 202 to diversify the causal relations represented in the dataset. To simulate realistic images in 3D scenes,
 203 we select or design causal relations to generate structured datasets and use Blender¹ to render high-
 204 quality images, as shown in Fig. 2. Furthermore, by introducing various views and backgrounds,
 205 CAUSAL3D presents the same scene in different surroundings, enhancing dataset diversity and con-
 206 textual richness.

3.1 DATASET COMPONENTS

208 **Physically Consistent Scenes** In the physically consistent setting, CAUSAL3D incorporates fun-
 209 fundamental physical principles, such as light dynamics, magnetic fields, water pressure, and mechan-
 210 ics, to ensure realistic causal relations. To systematically vary the complexity of causal discovery,
 211 we curated 8 distinct scenes, each featuring 2 to 5 variables with unique causal structures. Each
 212 scene contains 10K samples. We provide visual overviews of each scene in Appendix 6.

213 **Hypothetical Scenes** Since causal relations in reality are often complex and difficult to observe,
 214 designing scenes with diverse causal graphs is challenging. In CAUSAL3D, we also introduce addi-

¹<https://www.blender.org/>

tional hypothetical scenes that broaden the range of causal relations in our benchmark. Specifically, we explore causal relations under artificially defined hypothetical rules and synthesize causal relations among three fundamental 3D objects in Blender: sphere, cuboid, and cone. By defining specific dependencies among their variables (e.g., sphere radius, cuboid height), we construct both linear and non-linear causal relations across various graph configurations. This process yields 11 hypothetical scenes, each containing 10K samples. More details can be found in Appendix 6.

3.2 DATA CONSTRUCTION

The data construction process is shown in Fig. 2. The upper half shows the construction of real physical scenes. We first collect physical entities that exist in the real world, such as springs and magnets, etc. Then, we explore the physical laws within these entities and identify the corresponding causal graphs. Based on the causal graphs, we can generate tabular data, where each row represents a sample, and different columns correspond to different values of various variables. For variables without parents, we assign values randomly using a uniform distribution, while the values of other variables are calculated according to the causal graphs and physical laws. For example, if we select a spring and a block as our physical entities, the variables involved include the spring constant k , the deformation X , and the weight of the block W . The physical law governing these variables is Hooke’s Law: $X = W/k$. We can randomly assign values to W and k , and then calculate X accordingly. The generated tabular data can then be input into Blender to render multi-perspective scenes. It is worth noting that we have set a background switch to choose whether to use a real or virtual background.

The lower half of Fig. 2 displays the construction of hypothetical scenes. We first identify various dimensions of geometric bodies to serve as variables and then manually design the relations among these variables. The remaining steps are the same as those in generating physical scenes, with the only difference being that they do not include real backgrounds because the hypothetical objects and relations do not exist in the real world.

3.3 TASK DESIGNS

Based on our dataset, we focus on three key causal tasks to evaluate state-of-the-art algorithms and models in discovering and leveraging causal relations across diverse causal structures and scenes. We focus on the widely adopted setting of causal learning from observational data. These tasks include:

Causal discovery from tabular data This task focuses on identifying latent causal relations among variables using only tabular data. In this setting, we have high-level causal variable values recorded in the tabular data and do not rely on image information. It is evaluated based on the correctness of inferred causal structures across various datasets and underlying causal mechanisms.

Causal representation learning from images This task aims to learn disentangled and causally meaningful representations from images, meanwhile enabling models to capture underlying causal relations between high-level concepts. We use image data along with any additional information required by the models as input. Evaluation is based on generated images after intervening on learned representations, assessing whether they accurately reflect the corresponding causal variables and causal relations.

Causal discovery & intervention from few images This task focuses on uncovering causal relations and assessing intervention results with a limited number of images. Unlike traditional causal discovery methods that rely on large datasets, this task evaluates the ability of models to infer causal structures from a small set of images. Furthermore, we conduct causal interventions by manipulating a certain variable to observe its effect on the whole image. Causal intervention is often implemented with the do-operator $do(\cdot)$ (Pearl, 2009). Here, $do(X = x)$ means modifying a variable X to a specific value x while keeping all other influences unchanged. Intervention evaluation is based on whether the intervened images still remain consistent with the underlying causal relations.

270 **4 EVALUATIONS**
 271

272 **Overview.** In this section, we conduct a systematic evaluation on our benchmark Causal3D, focusing
 273 on three major causal tasks as aforementioned. For each task, we select appropriate models to
 274 assess their performance across diverse scenes. For causal discovery from tabular data, we evaluate
 275 traditional causal discovery methods alongside an LLM-based causal agent. For causal representa-
 276 tion learning, we benchmark state-of-the-art methods to examine their ability to extract meaningful
 277 causal factors. Lastly, for causal discovery and intervention from few images, we test various VLMs
 278 with different prompts. Our experiments span multiple settings with comprehensive insights.
 279

280 **4.1 EXPERIMENT SETTINGS**
 281

282 **Data Preprocessing.** Both image and tabular data were meticulously prepared to ensure seamless
 283 compatibility with the evaluated models. Image data were resized and normalized as required, and
 284 tabular data were formatted to meet the input specifications of traditional causal discovery methods.
 285

286 **Evaluation Metrics.** We mainly use two metrics to quantify the experimental results: **1) F1 Score**
 287 is used to evaluate causal discovery results, which represents the harmonic mean of precision and
 288 recall of discovered causal relations. **2) Accuracy** is used in causal intervention, which measures
 289 the fraction of consistent causal relations in the intervened image. Each experiment is repeated 10
 290 times per setting, and the final results are obtained by averaging these results for robust evaluation.
 291

292 **4.2 CAUSAL DISCOVERY FROM TABULAR DATA**
 293

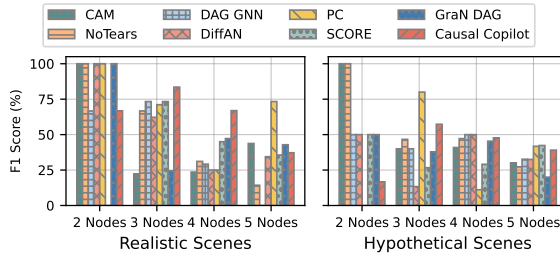
294 **Evaluated Methods.** We evaluate the
 295 performance of various causal discov-
 296 ery methods on tabular data, covering
 297 both traditional algorithms and emerging
 298 LLM-powered approaches. We assess
 299 7 traditional methods: CAM, NoTears,
 300 DAG GNN, DiffAN, PC, SCORE (Rol-
 301 land et al., 2022), and GraN DAG; 1 LLM-
 302 based method: Causal Copilot (Wang
 303 et al., 2024b). All experiments were con-
 304 ducted on an NVIDIA RTX 4090 GPU.
 305

306 **Results and Analysis.** The results are shown in Fig. 3. We test all methods on datasets representing
 307 both real and hypothetical scenes, categorized by causal graph complexity, ranging from 2- to 5-
 308 node structures. Each method takes the input of given tabular data and outputs a causal graph, and
 309 we compare it with the ground-truth causal graphs using the F1 score. The final evaluation metric
 310 is computed by averaging F1 scores within each node category. As shown in Fig. 3, although the
 311 performance of different methods varies within the same category, it can be observed in both realis-
 312 tic scenes and hypothetical scenes that there is a general downward trend in performance from 2-node
 313 to 5-node scenes. This aligns with our common sense and the laws of physics: the more variables
 314 there are in a scene, the more difficult it is to uncover the underlying rules.
 315

316 **4.3 CAUSAL REPRESENTATION LEARNING**
 317

318 **Evaluated Methods.** In this section, we evaluate causal representation learning models, including
 319 CausalVAE, DEAR, ICM-VAE (Komanduri et al., 2023), and CDG-VAE (An et al., 2023) on our
 320 dataset. The images and other information needed by models (e.g., CausalVAE requires annotations
 321 of causal variables) are taken as input. These methods are all based on the variational autoencoder
 322 (VAE) framework and aim to learn a low-dimensional representation composed of multiple disen-
 323 tangled yet causally related latent variables inside images.
 324

325 **Evaluation Strategy.** Since many of these models require a (partial) causal graph as input or
 326 supervision, it would be unfair to directly evaluate them with regular causal discovery metrics we
 327 used in the previous subsection. Following the evaluation strategy of previous works (Yang et al.,
 328 2020; Shen et al., 2022; Komanduri et al., 2023; An et al., 2023), we apply interventions on each
 329 variable separately by modifying its corresponding causal representations, and then decode the
 330 modified latent representation back to generate an intervened image. By assessing whether the
 331



332 **Figure 3:** Results of different causal discovery methods
 333 from tabular data on realistic/hypothetical scenes.
 334

causally related variables in the image change accordingly, we can evaluate whether the model has effectively learned the causal relations within our dataset.

Since these models only accept 2D images, we render the 3D scenes from a fixed viewpoint as inputs. For CausalVAE, DEAR, and ICM-VAE, we use *spring* and *seesaw* for evaluation. However, for CDG-VAE, which requires a structured mask to distinguish each object (i.e., variable), meaning that each object must move within a specific region, *spring* and *seesaw* do not satisfy this requirement. Therefore, we select *reflection* and *pendulum* for evaluation.

Results and Analysis. Intervention results are showcased in Fig. 4. For each given original image, we select a pair of “cause” and “result” variables to intervene with do-operation. For *spring*, the cause is the weight of the wooden block, and the result is the spring’s deformation. We first apply an intervention on the weight of the wooden block (cause), with the intervened image shown in the left-middle column. We observe that decreasing the block’s weight leads to a corresponding decrease in the spring’s deformation. This aligns with the causal relation, where the block’s weight directly influences the spring’s deformation. However, when we directly modify the spring’s deformation (result), as shown in the left-last column, the block’s weight remains unchanged. This confirms the unidirectional nature of causal relations, where the cause affects the effect, but not vice versa. The results for the *seesaw* scene exhibit a similar pattern. When we apply an intervention on the torque on the left side (cause), as shown in the right-middle column, the seesaw’s direction (result) reverses accordingly. However, when we directly intervene on the seesaw’s direction, the torque on both the left and right sides remains unchanged. Similar observations hold for *reflection*, where the incident light serves as the cause and the reflected light as the result, and for *pendulum*, where the pendulum’s angle acts as the cause, influencing the position and length of its shadow.

Although these models may not perform optimally in certain scenes, exhibiting distortions in reconstructed images and incomplete disentanglement of attributes, they still capture some underlying causal relations. This indicates the rationality of our proposed benchmark and highlights the need for further research in achieving more effective causal representation learning from images.

4.4 CAUSAL DISCOVERY FROM FEW IMAGES

Evaluated Methods. Unlike traditional causal discovery methods that rely on tabular data or large-scale training images, we leverage pretrained VLMs to perform causal discovery using a small number of images. In this section we use ChatGPT², Gemini³ and Claude⁴ to discover causal relations by few image examples and textual prompts in real and hypothetical scenes. The VLMs are tasked with uncovering causal relations by generating adjacency matrices representing causal graphs. Each prompt specifies key variables in the scenes, explicitly guiding the models to infer causal structures. We use 4 different prompting strategies, as detailed in Tab. 5 in the Appendix 7.

- 1) Basic Prompts:** General instructions that broadly guide the models to identify causal relations.
- 2) Explicit Function Prompts:** The model is designated as a causal discovery expert to identify causal relationships among image variables.
- 3) Chain of Thought (CoT):** The model is prompted to reason through the causal discovery process step by step without any prior examples. This approach encourages structured reasoning and provides insights into how the model interprets causal relations.

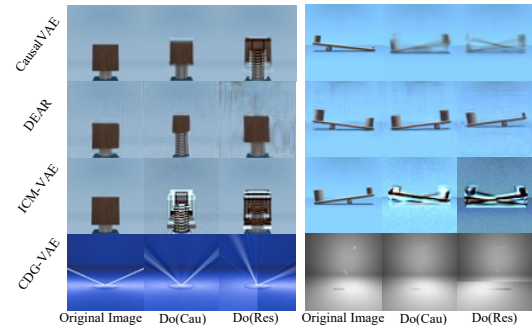


Figure 4: Examples of the 4 causal representation learning model results. In each scene, the 3 columns show: 1) original images, 2) Do(Cau): results after intervening on a “cause” variable, and 3) Do(Res): after intervening on a “result” variable.

We observe that decreasing the block’s weight leads to a corresponding decrease in the spring’s deformation. This aligns with the causal relation, where the block’s weight directly influences the spring’s deformation. However, when we directly modify the spring’s deformation (result), as shown in the left-last column, the block’s weight remains unchanged. This confirms the unidirectional nature of causal relations, where the cause affects the effect, but not vice versa. The results for the *seesaw* scene exhibit a similar pattern. When we apply an intervention on the torque on the left side (cause), as shown in the right-middle column, the seesaw’s direction (result) reverses accordingly. However, when we directly intervene on the seesaw’s direction, the torque on both the left and right sides remains unchanged. Similar observations hold for *reflection*, where the incident light serves as the cause and the reflected light as the result, and for *pendulum*, where the pendulum’s angle acts as the cause, influencing the position and length of its shadow.

Although these models may not perform optimally in certain scenes, exhibiting distortions in reconstructed images and incomplete disentanglement of attributes, they still capture some underlying causal relations. This indicates the rationality of our proposed benchmark and highlights the need for further research in achieving more effective causal representation learning from images.

²<https://platform.openai.com/docs/api-reference/introduction>

³<https://ai.google.dev/api?lang=python>

⁴<https://www.anthropic.com/api>

378
 379 **4) Few-Shot:** The model is given three exemplar
 380 cases of causal discovery before performing the
 381 task, enabling it to generalize better by leveraging
 382 prior examples to improve causal relation identi-
 383 fication. Performance is evaluated by comparing
 384 the generated adjacency matrices with the ground
 385 truth, providing a quantitative measure of the causal
 386 discovery task.

386 **Results and Analysis.** Demonstrated in Fig. 5(a),
 387 models performed significantly better in real-world
 388 scenes (e.g., governed by Hooke’s Law, magnetic
 389 fields and etc.) compared to hypothetical scenes,
 390 benefiting from prior physical knowledge embedded
 391 in their LLM components. However, as causal
 392 relations became more complex and involved more
 393 variables, performance declined, highlighting the
 394 challenge of uncovering causality in such scenes. In the hypothetical scenes, as shown
 395 in Fig. 5(b), reveal poor performance. This suggests that when prior real-world knowledge is
 396 unavailable and only a limited number of images are provided, models consistently fail to uncover
 397 latent causal relations. Consequently, current closed-source VLMs have been shown to be unreliable
 398 for causal discovery in hypothetical settings.

399 Views and Backgrounds.

400 CAUSAL3D provides multi-view
 401 images of the same scene, simulating
 402 real-world 3D environments with both
 403 virtual and realistic backgrounds.
 404 This enables in-depth analysis of how
 405 different viewpoints and background
 406 contexts affect causal discovery
 407 performance. Case studies from
 408 the Spring and Parabola scenes are
 409 shown in Fig. 6. Within the ex-
 410 periments, different 3D views affect
 411 the performance in causal discovery.
 412 Interestingly, our results reveal that
 413 intuitive views, such as a front view,
 414 are not always the most effective for
 415 uncovering latent causality. Different
 416 viewpoints can either increase or
 417 decrease task difficulty, with no single
 418 “golden standard” view for causal
 419 discovery. Additionally, when comparing
 420 multi-view and single-view inputs in
 421 the causal discovery task, multi-view
 422 performance varies depending on the
 423 scene (as shown in Fig. 9). In scenes
 424 with simple causal relations (e.g., a
 425 spring system with a linear relation among
 426 three variables), multi-view inputs tend to degrade model
 427 performance, possibly introducing unnecessary noise. Conversely, in more complex 3D scenes
 428 with intricate causal dependencies, like a parabola scene involving nonlinear relations among
 429 four variables in the virtual background, multi-view perspectives enhance inference accuracy, suggesting
 430 that additional viewpoints help capture richer causal structures in such settings.

431 Comparing virtual and realistic backgrounds, we find that realistic backgrounds introduce additional
 432 noise, making causal discovery more challenging. Our experiments indicate that even when models
 433 leverage prior real-world knowledge encoded in LLMs, the presence of realistic background
 434 information increases task complexity and negatively impacts inference performance (quantitative
 435 results shown in Fig. 37 in Appendix 7).

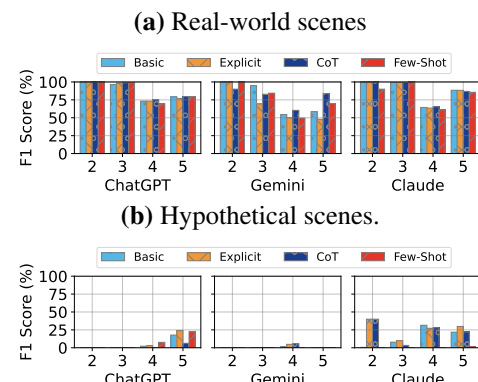


Figure 5: Causal discovery results of VLMs in various scenes, averaged over datasets with 2–5 nodes in the causal graph.

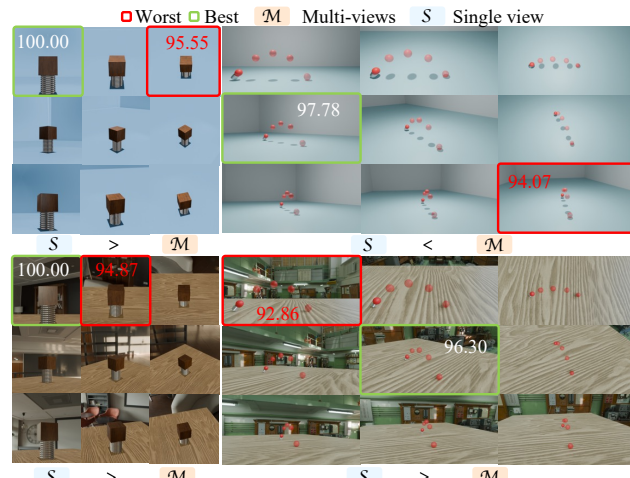
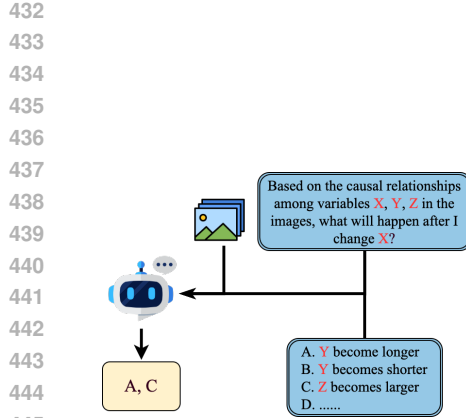


Figure 6: **Spring** and **Parabola** scene. Using the F1 score as metric, we assess VLM performance in causal discovery. The **best** and **worst** views are highlighted to demonstrate the impact of different views. To analyze the effect of multi-view vs. single-view images, we average the performance across 9 individual views in each scene and compare it with the overall multi-view performance. Details and concrete numerical results are provided in Appendix 7.2.



446 Figure 7: Example of intervention
447 prompts for trained VLMs.
448

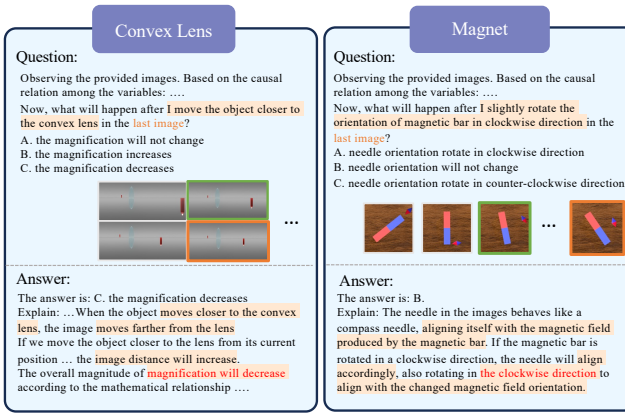
449 4.5 CAUSAL INTERVENTION IN VLMs

450
451 **Evaluated Methods.** To further assess the ability to learn causality from images, causal intervention
452 serves as a crucial step beyond causal discovery. In this experiment, we leverage VLMs in
453 interventions. This task is formulated as a multiple-choice problem, where the model must identify
454 the correct outcomes based on induced causal changes. The detailed inference pipeline is illustrated
455 in Fig. 7. In this setup, VLMs are provided with a few images along with questions about the
456 variables present in the scene. By posing queries such as “*What will happen after changing variable*
457 *X?*”, we expect the model to return the correct answer based on the causal relations depicted in
458 the given images. This evaluation determines whether VLMs genuinely comprehend and reason
459 causal relations rather than relying solely on statistical patterns. In this experiment, intervention
460 performance is measured by model selection accuracy. We evaluate 3 popular commercial VLMs
461 on this task: ChatGPT-4o, Gemini-1.5-Pro, and Claude-3.5-Haiku⁵.

462 **Results and Analysis.** As shown in
463 Tab. 2, our experiments indicate that
464 current VLMs struggle to handle complex
465 rules, e.g. magnetic fields, in causal
466 intervention tasks. We found that the
467 models’ inferences are dominated by the
468 prior knowledge embedded in the LLMs,
469 while visual cues—despite containing the
470 ground truth—are largely ignored (see Fig. 8).

471 5 CONCLUSION

472 CAUSAL3D is a comprehensive benchmark designed to evaluate causal reasoning in visual AI,
473 including causal tasks of discovery, disentanglement, and intervention. Our dataset integrates
474 structured causal graphs with corresponding 3D visual representations, providing a rigorous
475 assessment framework across diverse physical and hypothetical scenes. Experimental results
476 demonstrate that: 1) the performance of current causal discovery algorithms decreases as the
477 increasing of the complexity of causal structures; 2) for causal representation learning, the current
478 state-of-arts can not well handle our realistic and diverse 3D scenes; 3) commercial VLMs struggle
479 with causal inference based on visual cues and complex scenarios, particularly in hypothetical
480 settings where prior knowledge is absent. CAUSAL3D serves as a critical step toward bridging the
481 gap between traditional causal research and computer vision, enabling a more comprehensive and
482 fine-grained evaluation of causal inference. We envision CAUSAL3D as a foundation for future
483 research, fostering advancements in causal-aware AI models and driving progress toward more
484 reliable and interpretable machine intelligence.



446 Figure 8: Case studies of failures. VLMs fail to grasp
447 causality within physically consistent scenes for intervention
448 tasks.

5 Table 2: Causal intervention in VLMs: Evaluation using three real-world rules, with accuracy (%) reported.

Models	Reflection	Lens	Mag. Field
ChatGPT	96.67	100.00	50.00
Gemini	100.00	100.00	0.00
Claude	100.00	96.67	13.33

⁵Model versions are those publicly available as of January 2025.

486
487
ETHICS STATEMENT488
489
490
491
492
493
494
495
This research adheres to the ICLR Code of Ethics. The study does not involve human subjects,
496 personally identifiable information, or sensitive data. All datasets used are publicly available, and
497 appropriate steps were taken to ensure compliance with privacy, fairness, and research integrity
498 standards. No conflicts of interest or ethical concerns are anticipated.499
500
REPRODUCIBILITY STATEMENT501
502
503
504
505
506
507
508
509
510
We conducted extensive experiments with multiple random seeds to ensure the robustness and re-
511 producibility of our results. Detailed descriptions of model architectures, training procedures, and
512 hyperparameters closely follow those reported in the original baseline papers. The data generation
513 code is submitted in a zip file as supplementary materials.514
515
REFERENCES516
517
518
519
520
521
522
523
524
525
526
527
528
529
530
531
532
533
534
535
536
537
538
539
SeungHwan An, Kyungwoo Song, and Jong-June Jeon. Causally disentangled generative variational
510 autoencoder. In *ECAI 2023*, pages 93–100. IOS Press, 2023.511
512
513
514
515
516
517
518
519
520
521
522
523
524
525
526
527
528
529
530
531
532
533
534
535
536
537
538
539
Tayfun Ates, M. Ateşoğlu, Çağatay Yigit, İlker Keser, Mert Kobas, Erkut Erdem, Aykut Erdem,
510 Tilbe Goksun, and Deniz Yuret. CRAFT: A benchmark for causal reasoning about forces and
511 interactions. In Smaranda Muresan, Preslav Nakov, and Aline Villavicencio, editors, *Findings
512 of the Association for Computational Linguistics: ACL 2022*, pages 2602–2627, Dublin, Ireland,
513 May 2022. Association for Computational Linguistics. doi: 10.18653/v1/2022.findings-acl.205.
514 URL <https://aclanthology.org/2022.findings-acl.205/>.515
516
517
518
519
520
521
522
523
524
525
526
527
528
529
530
531
532
533
534
535
536
537
538
539
Taiyu Ban, Lyvzhou Chen, Xiangyu Wang, and Huanhuan Chen. From query tools to causal archi-
510 tects: Harnessing large language models for advanced causal discovery from data, 2023. URL
511 <https://arxiv.org/abs/2306.16902>.512
513
514
515
516
517
518
519
520
521
522
523
524
525
526
527
528
529
530
531
532
533
534
535
536
537
538
539
Peter Bühlmann, Jonas Peters, and Jan Ernest. Cam: Causal additive models, high-dimensional order
510 search and penalized regression. *The Annals of Statistics*, 42(6), December 2014. ISSN 0090-
511 5364. doi: 10.1214/14-aos1260. URL <http://dx.doi.org/10.1214/14-AOS1260>.512
513
514
515
516
517
518
519
520
521
522
523
524
525
526
527
528
529
530
531
532
533
534
535
536
537
538
539
Maria Victoria Carro, Francisca Gauna Selasco, Denise Alejandra Mester, Margarita Gonzales,
510 Mario A. Leiva, Maria Vanina Martinez, and Gerardo I. Simari. Do large language models show
511 biases in causal learning?, 2024. URL <https://arxiv.org/abs/2412.10509>.512
513
514
515
516
517
518
519
520
521
522
523
524
525
526
527
528
529
530
531
532
533
534
535
536
537
538
539
David Maxwell Chickering. Learning equivalence classes of bayesian-network structures. *The
510 Journal of Machine Learning Research*, 2:445–498, 2002.511
512
513
514
515
516
517
518
519
520
521
522
523
524
525
526
527
528
529
530
531
532
533
534
535
536
537
538
539
Martina Cinquini, Fosca Giannotti, and Riccardo Guidotti. Boosting synthetic data generation with
510 effective nonlinear causal discovery. In *2021 IEEE Third International Conference on Cognitive
511 Machine Intelligence (CogMI)*, pages 54–63. IEEE, 2021.512
513
514
515
516
517
518
519
520
521
522
523
524
525
526
527
528
529
530
531
532
533
534
535
536
537
538
539
Zizhen Deng, Xiaolong Zheng, Hu Tian, and Daniel Dajun Zeng. Deep causal learning: representa-
510 tion, discovery and inference. *arXiv preprint arXiv:2211.03374*, 2022.511
512
513
514
515
516
517
518
519
520
521
522
523
524
525
526
527
528
529
530
531
532
533
534
535
536
537
538
539
Alexey Dosovitskiy, Lucas Beyer, Alexander Kolesnikov, Dirk Weissenborn, Xiaohua Zhai, Thomas
510 Unterthiner, Mostafa Dehghani, Matthias Minderer, Georg Heigold, Sylvain Gelly, Jakob Uszko-
511 reit, and Neil Houlsby. An image is worth 16x16 words: Transformers for image recogni-
512 tion at scale. In *International Conference on Learning Representations (ICLR)*, 2021. URL
513 <https://openreview.net/forum?id=YicbFdNTTy>.514
515
516
517
518
519
520
521
522
523
524
525
526
527
528
529
530
531
532
533
534
535
536
537
538
539
Yuxin Fang, Wen Wang, Binhui Xie, Quan Sun, Ledell Wu, Xinggang Wang, Tiejun Huang, Xinlong
510 Wang, and Yue Cao. EVA: Exploring the limits of masked visual representation learning at scale.
511 In *Proceedings of the IEEE/CVF Conference on Computer Vision and Pattern Recognition*, pages
512 19358–19369, 2023.

540 Zhijing Jin, Yuen Chen, Felix Leeb, Luigi Gresele, Ojasv Kamal, Zhiheng Lyu, Kevin Blin, Fer-
 541 nando Gonzalez Adaucto, Max Kleiman-Weiner, Mrinmaya Sachan, et al. Cladder: A benchmark
 542 to assess causal reasoning capabilities of language models. *Advances in Neural Information Pro-*
 543 *cessing Systems*, 36, 2024.

544 Thomas Jiralerspong, Xiaoyin Chen, Yash More, Vedant Shah, and Yoshua Bengio. Efficient
 545 causal graph discovery using large language models, 2024. URL <https://arxiv.org/abs/2402.01207>.

546 Emre Kıcıman, Robert Ness, Amit Sharma, and Chenhao Tan. Causal reasoning and large language
 547 models: Opening a new frontier for causality. *arXiv preprint arXiv:2305.00050*, 2023.

548 Aneesh Komanduri, Yongkai Wu, Feng Chen, and Xintao Wu. Learning causally disentangled repre-
 549 sentations via the principle of independent causal mechanisms. *arXiv preprint arXiv:2306.01213*,
 550 2023.

551 Sébastien Lachapelle, Philippe Brouillard, Tristan Deleu, and Simon Lacoste-Julien. Gradient-based
 552 neural dag learning, 2020. URL <https://arxiv.org/abs/1906.02226>.

553 Xiaoyu Liu, Paiheng Xu, Junda Wu, Jiaxin Yuan, Yifan Yang, Yuhang Zhou, Fuxiao Liu, Tianrui
 554 Guan, Haoliang Wang, Tong Yu, Julian McAuley, Wei Ai, and Furong Huang. Large language
 555 models and causal inference in collaboration: A comprehensive survey, 2024a. URL <https://arxiv.org/abs/2403.09606>.

556 Xiaoyu Liu, Paiheng Xu, Junda Wu, Jiaxin Yuan, Yifan Yang, Yuhang Zhou, Fuxiao Liu, Tianrui
 557 Guan, Haoliang Wang, Tong Yu, et al. Large language models and causal inference in collabora-
 558 tion: A comprehensive survey. *arXiv preprint arXiv:2403.09606*, 2024b.

559 Yang Liu, Yu-Shen Wei, Hong Yan, Guan-Bin Li, and Liang Lin. Causal reasoning meets visual
 560 representation learning: A prospective study. *Machine Intelligence Research*, 19(6):485–511,
 561 2022.

562 Ze Liu, Yutong Lin, Yue Cao, Han Hu, Yixuan Wei, Zheng Zhang, Stephen Lin, and Baining Guo.
 563 Swin transformer: Hierarchical vision transformer using shifted windows. In *Proceedings of the*
 564 *IEEE/CVF International Conference on Computer Vision (ICCV)*, pages 10012–10022, 2021. doi:
 565 10.1109/ICCV48922.2021.00986.

566 Ziwei Liu, Ping Luo, Xiaogang Wang, and Xiaoou Tang. Deep learning face attributes in the
 567 wild. In *Proceedings of the IEEE International Conference on Computer Vision (ICCV)*, pages
 568 3730–3738, 2015. doi: 10.1109/ICCV.2015.425. URL <http://mmlab.ie.cuhk.edu.hk/projects/CelebA.html>.

569 Jing Ma. Causal inference with large language model: A survey. *arXiv preprint arXiv:2409.09822*,
 570 2024.

571 J. Mao, X. Yang, X. Zhang, N. Goodman, and J. Wu. Clevrer-humans: Describing physical and
 572 causal events the human way. In *Advances in Neural Information Processing Systems*, volume 35,
 573 pages 7755–7768, 2022.

574 Judea Pearl. *Causality*. Cambridge university press, 2009.

575 Atul Rawal, Adrienne Raglin, Qianlong Wang, and Ziying Tang. Investigating causal reasoning in
 576 large language models. In *Causality and Large Models @NeurIPS 2024*, 2024. URL <https://openreview.net/forum?id=EGWrfirmIM>.

577 Paul Rolland, Volkan Cevher, Matthäus Kleindessner, Chris Russell, Dominik Janzing, Bernhard
 578 Schölkopf, and Francesco Locatello. Score matching enables causal discovery of nonlinear ad-
 579 ditive noise models. In *International Conference on Machine Learning*, pages 18741–18753.
 580 PMLR, 2022.

581 Jakob Runge. Causal network reconstruction from time series: From theoretical assumptions to
 582 practical estimation. *Chaos: An Interdisciplinary Journal of Nonlinear Science*, 28(7):075310,
 583 2018. doi: 10.1063/1.5025050. URL <https://doi.org/10.1063/1.5025050>.

594 Jakob Runge, Sebastian Bathiany, Erik Boltt, Gustau Camps-Valls, Dim Coumou, Ethan Deyle,
 595 Clark Glymour, Marlene Kretschmer, Miguel D Mahecha, Jordi Muñoz-Marí, et al. Inferring
 596 causation from time series in earth system sciences. *Nature communications*, 10(1):1–13, 2019a.
 597

598 Jakob Runge, Peer Nowack, Marlene Kretschmer, Seth Flaxman, and Dino Sejdinovic. Detecting
 599 and quantifying causal associations in large nonlinear time series datasets. *Science Advances*, 5
 600 (11):eaau4996, 2019b. doi: 10.1126/sciadv.aau4996. URL <https://www.science.org/doi/10.1126/sciadv.aau4996>.

602 Fabrizio Russo and Francesca Toni. Causal discovery and knowledge injection for contestable neural
 603 networks (with appendices), 2023. URL <https://arxiv.org/abs/2205.09787>.

604

605 Pedro Sanchez, Xiao Liu, Alison Q O’Neil, and Sotirios A. Tsaftaris. Diffusion models for causal
 606 discovery via topological ordering, 2023. URL <https://arxiv.org/abs/2210.06201>.

607

608 Bernhard Schölkopf. Causality for machine learning. In *Probabilistic and causal inference: The
 609 works of Judea Pearl*, pages 765–804. 2022.

610

611 Bernhard Schölkopf, Francesco Locatello, Stefan Bauer, Nan Rosemary Ke, Nal Kalchbrenner,
 612 Anirudh Goyal, and Yoshua Bengio. Toward causal representation learning. *Proceedings of
 613 the IEEE*, 109(5):612–634, 2021.

614

615 ChengAo Shen, Zhengzhang Chen, Dongsheng Luo, Dongkuan Xu, Haifeng Chen, and Jingchao Ni.
 616 Exploring multi-modal integration with tool-augmented llm agents for precise causal discovery.
 617 *arXiv preprint arXiv:2412.13667*, 2024.

618

619 Xinwei Shen, Furui Liu, Hanze Dong, Qing Lian, Zhitang Chen, and Tong Zhang. Weakly super-
 620 vised disentangled generative causal representation learning, 2022. URL <https://arxiv.org/abs/2010.02637>.

621

622 Mannat Singh, Laura Gustafson, Aaron Adcock, Vinicius de Freitas Reis, Bugra Gedik, Raj Prateek
 623 Kosaraju, Dhruv Mahajan, Ross Girshick, Piotr Dollár, and Laurens van der Maaten. Revisiting
 624 weakly supervised pre-training of visual perception models. In *Proceedings of the IEEE/CVF
 625 Conference on Computer Vision and Pattern Recognition*, pages 804–814, 2022.

626

627 Peter Spirtes, Clark Glymour, and Richard Scheines. *Causation, Prediction, and Search*. MIT Press,
 2nd edition, 2000a. ISBN 978-0262194402.

628

629 Peter Spirtes, Clark N Glymour, and Richard Scheines. *Causation, prediction, and search*. MIT
 630 press, 2000b.

631

632 Ruibo Tu, Zineb Senane, Lele Cao, Cheng Zhang, Hedvig Kjellström, and Gustav Eje Henter.
 633 Causality for tabular data synthesis: A high-order structure causal benchmark framework, 2024.
 634 URL <https://arxiv.org/abs/2406.08311>.

635

636 H. Y. Tung, M. Ding, Z. Chen, D. Bear, C. Gan, J. Tenenbaum, and K. Smith. Physion++: Evaluating
 637 physical scene understanding that requires online inference of different physical properties. In
 638 *Advances in Neural Information Processing Systems*, volume 36, 2024.

639

640 J. Von Kügelgen, Y. Sharma, L. Greselle, W. Brendel, B. Schölkopf, M. Besserve, and F. Locatello.
 641 Self-supervised learning with data augmentations provably isolates content from style. In *Ad-
 642 vances in Neural Information Processing Systems*, volume 34, pages 16451–16467, 2021.

643

644 Guangya Wan, Yuqi Wu, Mengxuan Hu, Zhixuan Chu, and Sheng Li. Bridging causal discovery and
 645 large language models: A comprehensive survey of integrative approaches and future directions,
 2024. URL <https://arxiv.org/abs/2402.11068>.

646

647 Liuyi Wang, Zongtao He, Ronghao Dang, Mengjiao Shen, Chengju Liu, and Qijun Chen. Vision-
 648 and-language navigation via causal learning. In *Proceedings of the IEEE/CVF Conference on
 649 Computer Vision and Pattern Recognition*, pages 13139–13150, 2024a.

648 Wenhai Wang, Jifeng Dai, Zhe Chen, Zhenhang Huang, Zhiqi Li, Xizhou Zhu, Xiaowei Hu, Tong
 649 Lu, Lewei Lu, Hongsheng Li, Xiaogang Wang, and Yu Qiao. Internimage: Exploring large-
 650 scale vision foundation models with deformable convolutions. In *Proceedings of the IEEE/CVF*
 651 *Conference on Computer Vision and Pattern Recognition*, pages 14408–14419, 2023. doi: 10.
 652 1109/CVPR52729.2023.01440.

653 Xinyue Wang, Kun Zhou, Wenyi Wu, Fang Nan, and Biwei Huang. Causal-copilot: An autonomous
 654 causal analysis agent. 2024b.

655 Bingyang Wen, Luis Oliveros Colon, K. P. Subbalakshmi, and R. Chandramouli. Causal-tgan:
 656 Generating tabular data using causal generative adversarial networks, 2021. URL <https://arxiv.org/abs/2104.10680>.

657 Bingyang Wen, Yupeng Cao, Fan Yang, Koduvayur Subbalakshmi, and Rajarathnam Chandramouli.
 658 Causal-tgan: Modeling tabular data using causally-aware gan. In *ICLR Workshop on Deep Gen-
 erative Models for Highly Structured Data*, 2022.

659 Anpeng Wu, Kun Kuang, Minqin Zhu, Yingrong Wang, Yujia Zheng, Kairong Han, Baohong Li,
 660 Guangyi Chen, Fei Wu, and Kun Zhang. Causality for large language models, 2024. URL
 661 <https://arxiv.org/abs/2410.15319>.

662 Mengyue Yang, Furui Liu, Zhitang Chen, Xinwei Shen, Jianye Hao, and Jun Wang. Causalvae:
 663 Structured causal disentanglement in variational autoencoder, 2023. URL <https://arxiv.org/abs/2004.08697>.

664 Muyu Yang, Feng Liu, Zhi Chen, Xi Shen, Jie Hao, and Jianmin Wang. Causalvae: Structured
 665 causal disentanglement in variational autoencoder. *arXiv preprint arXiv:2004.08697*, 2020. URL
 666 <https://arxiv.org/abs/2004.08697>.

667 Tian-Le Yang, Kuang-Yao Lee, Kun Zhang, and Joe Suzuki. Functional linear non-gaussian acyclic
 668 model for causal discovery, 2024. URL <https://arxiv.org/abs/2401.09641>.

669 Xu Yang, Hanwang Zhang, Guojun Qi, and Jianfei Cai. Causal attention for vision-language tasks.
 670 In *Proceedings of the IEEE/CVF conference on computer vision and pattern recognition*, pages
 671 9847–9857, 2021.

672 Zhuolin Yang, Zhikuan Zhao, Boxin Wang, Jiawei Zhang, Linyi Li, Hengzhi Pei, Bojan Karlaš,
 673 Ji Liu, Heng Guo, Ce Zhang, et al. Improving certified robustness via statistical learning with
 674 logical reasoning. *Advances in Neural Information Processing Systems*, 35:34859–34873, 2022.

675 Yue Yu, Jie Chen, Tian Gao, and Mo Yu. Dag-gnn: Dag structure learning with graph neural
 676 networks, 2019. URL <https://arxiv.org/abs/1904.10098>.

677 Shitian Zhao, Zhuowan Li, Yadong Lu, Alan Yuille, and Yan Wang. Causal-cog: A causal-effect
 678 look at context generation for boosting multi-modal language models. In *Proceedings of the
 679 IEEE/CVF Conference on Computer Vision and Pattern Recognition*, pages 13342–13351, 2024.

680 Xun Zheng, Bryon Aragam, Pradeep Ravikumar, and Eric P. Xing. Dags with no tears: Continu-
 681 ous optimization for structure learning. In *Advances in Neural Information Processing Systems*,
 682 volume 31, pages 9472–9483, 2018. URL <https://papers.nips.cc/paper/2018/hash/e347c51419ffb23ca3fd5050202f9c3d-Abstract.html>.

683 Robin S Zimmermann, Yash Sharma, Steffen Schneider, Matthias Bethge, and Wieland Brendel.
 684 Contrastive learning inverts the data generating process. In *Proceedings of the International
 685 Conference on Machine Learning (ICML)*, pages 12979–12990. PMLR, July 2021.

686

687

688

689

690

691

692

693

694

695

696

697

698

699

700

701

APPENDIX

In the appendix, we will provide the statistics of Causal3D and supplement the scenes and their data details that were not presented in the main text. Additionally, we will also display the remaining experiment setups and results.

6 DATASET DETAILS AND ADDITIONAL SCENES

Causal3D is annotated with causal graphs that vary in node count and graph structure. For a global overview of Causal3D, we summarize the **number of settings** and the **number of causal structures** under different numbers of variables in each scene in Tab. 3a and Tab. 3b.

Fig. 9, Fig. 10, and Fig. 11 show the dataset details of different scenes, including the following information: name of scenes, the number of causal variables (i.e., nodes in causal graph), the relation types (linear or non-linear), causal graphs, and structural equations. For realistic scenes, we also add a brief description. Furthermore, we showcase all the scenes by randomly sampling 2D images from different viewpoints and surroundings for illustration (shown from Fig. 12 to Fig. 36). For notational simplicity, we omit the exogenous noise variables in the structural equations, all of which follow uniform distributions. For example, in the Reflection scene, the expression $A = B$ is a shorthand for the structural equation $B = A + \epsilon$, where ϵ is an independent uniform noise term. This non-Gaussianity ensures the identifiability of the causal direction $A \rightarrow B$.

Scene	Description	Causal Graph	Structure Equation
Reflection, Linear	<i>Light reflects off a mirror.</i>		A: Incident light. B: Outgoing light. $A = B$
Seesaw, Non-Linear	<i>A seesaw with a cylinder on each end.</i>		A: Left torque. B: Right torque. C: Seesaw tilt direction. $C = \text{sign}(A - B)$
Convex Lens, Non-Linear	<i>A candle and its image formed by a convex lens.</i>		A: Distance from lens to the object. B: Distance from the lens to the image. C: Magnification factor. $\frac{1}{f} = \frac{1}{A} + \frac{1}{B} \quad f \text{ is the focal length, which is a constant.}$ $C = -\frac{A}{B}$
Magnet, Non-Linear	<i>A magnet and a needle displaying its magnetic field.</i>		A: Rotation angle of the bar magnet. B: The x-coordinate of the magnetic needle. C: The y-coordinate of the magnetic needle. D: Orientation of the magnetic field at the needle. $D = \frac{\mu_0}{4\pi} \left(\frac{3(B, C)\vec{A}(B, C)}{(B, C)^5} - \frac{\vec{A}}{(B, C)^3} \right)$
Pendulum, Non-Linear	<i>A light source, a pendulum, and its shadow.</i>		A: Light position. B: Pendulum angle. C: Pendulum length. D: Shadow middle point position. E: Shadow length. $D = \frac{1}{2} \left(-\frac{y_l x_p + y_l C \sin B + A C \cos B - y_p A}{y_p - C \cos B - y_l} - \frac{y_l x_p - y_p A}{y_p - y_l} \right)$ $E = \frac{y_l x_p + y_l C \sin B + A C \cos B - y_p A}{y_p - C \cos B - y_l} + \frac{y_l x_p + y_l C \sin B + A C \cos B - y_p A}{y_p - C \cos B - y_l}$ (x_p, y_p) is the coordinate of the pendulum end point. y_l is the y-coordinate of the light.

Figure 9: Data details of realistic scenes (as a supplement to Fig. 1).

756
757
758
759
760
761

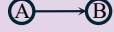
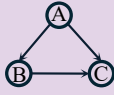
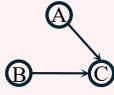
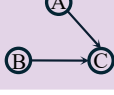
Scene	Causal Graph	Structure Equation
2 Variables, Linear		A: Volume of the ball. B: Volume of the cube. $B = 1.5A$
2 Variables, Non-Linear		A: Volume of the ball. B: Volume of the cube. $B = \cos(A)$
3 Variables, Fully Connected, Linear		A: Volume of the ball. B: Height of the cuboid. C: Base area of the cone. $B = 4A$ $C = -10A + 10B$
3 Variables, V-Structure, Linear		A: Volume of the ball. B: Height of the cuboid. C: Base area of the cone. $C = 0.4A + 0.7B$
3 Variables, V-Structure, Non-Linear		A: Volume of the ball. B: Height of the cuboid. C: Base area of the cone. $C = \tan(A) + 0.7B$

Figure 10: Data details of hypothetical scenes (2 variables and 3 variables).

786
787
788
789
790
791
792
793
794
795
796
797

# Nodes	2	3	4	5
Realistic	2	2	2	2
Hypothetical	2	3	3	3

802 (a) Number of settings per node count.

# Nodes	2	3	4	5
Realistic	1	2	2	2
Hypothetical	1	2	2	2

803 (b) Number of causal structures per node count.

804
805
806
807
808
809

Table 3: The basic statistic of Causal3D

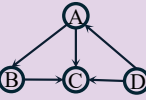
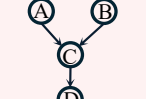
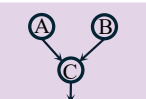
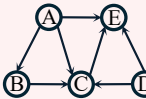
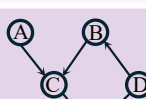
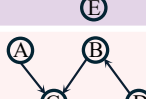
Scene	Causal Graph	Structure Equation
4 Variables, No V-structure Linear		<p>A: Volume of the ball. B: Volume of the cube. C: Base area of the cuboid. D: Base area of the cone.</p> $A = 0.5D$ $B = 0.3A$ $C = 0.4A + 0.6B + 0.9B$
4 Variables, V-Structure, Linear		<p>A: Volume of the ball. B: Volume of the cube. C: Base area of the cuboid. D: Base area of the cone.</p> $C = 0.3A + 0.7B$ $D = 0.4C$
4 Variables, V-Structure, Non-Linear		<p>A: Volume of the ball. B: Volume of the cube. C: Base area of the cuboid. D: Base area of the cone.</p> $C = 50 \sin(A) + 20B$ $D = 1100 \cos(C)$
5 Variables, No V-structure Linear		<p>A: Volume of the ball. B: Volume of the cube. C: Base area of the cuboid. D: Base area of the cone. E: Height of the cone.</p> $B = 0.01A$ $C = -0.01A + 16B$ $D = 1.2C$ $E = 5A - 0.5C + 2D$
5 Variables, V-Structure, Linear		<p>A: Volume of the ball. B: Volume of the cube. C: Base area of the cuboid. D: Base area of the cone. E: Height of the cone.</p> $B = 0.045D$ $C = 0.03A + 10B$ $E = 0.01C + 0.02D$
5 Variables, V-Structure, Non-Linear		<p>A: Volume of the ball. B: Volume of the cube. C: Base area of the cuboid. D: Base area of the cone. E: Height of the cone.</p> $B = 60 \sin(D)$ $C = 400 \cos(A) + 20B$ $E = 35 \tan(C) + 0.1D$

Figure 11: Data details of hypothetical scenes (4 variables and 5 variables).

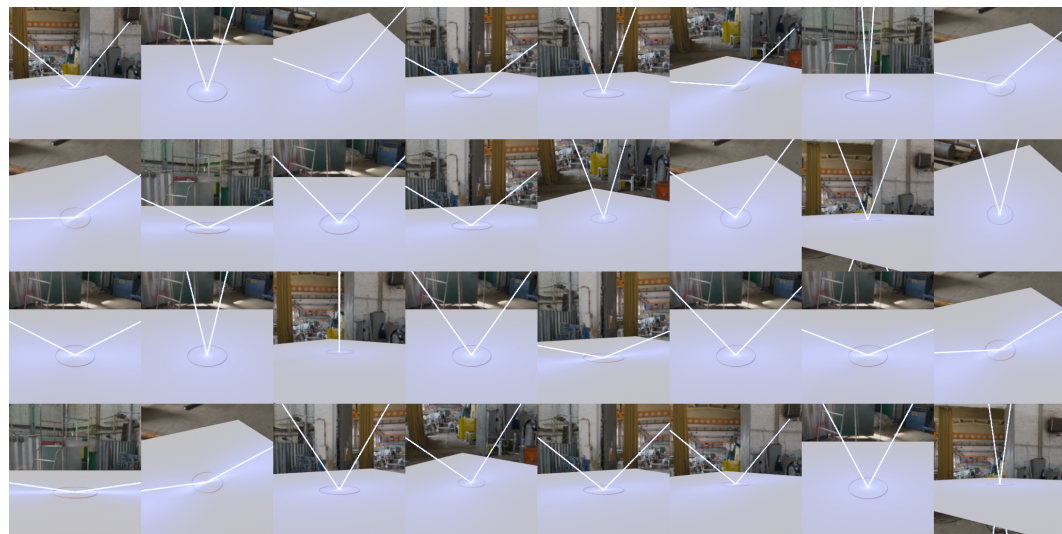


Figure 12: Reflection (Real Background).



Figure 13: Reflection (Virtual Background).

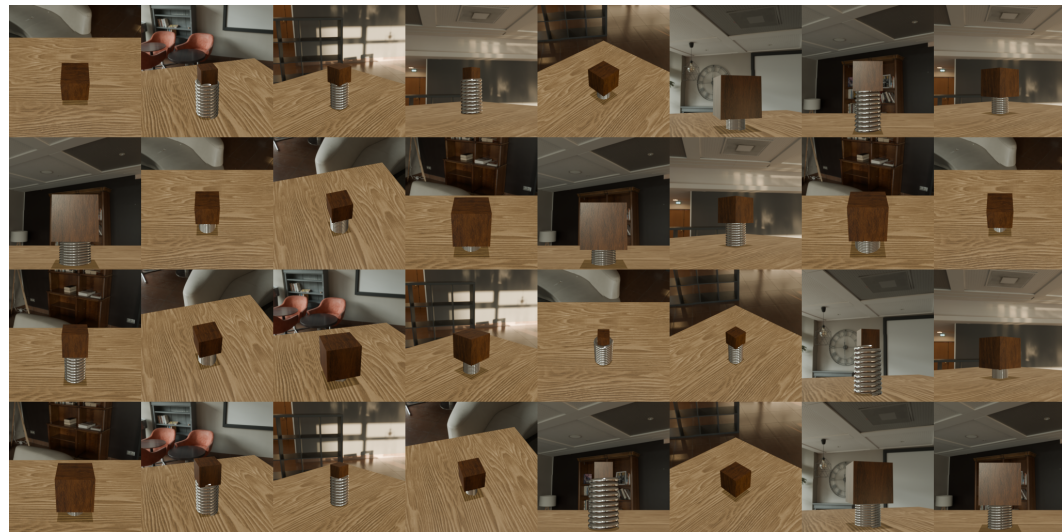


Figure 14: Spring (Real Background).

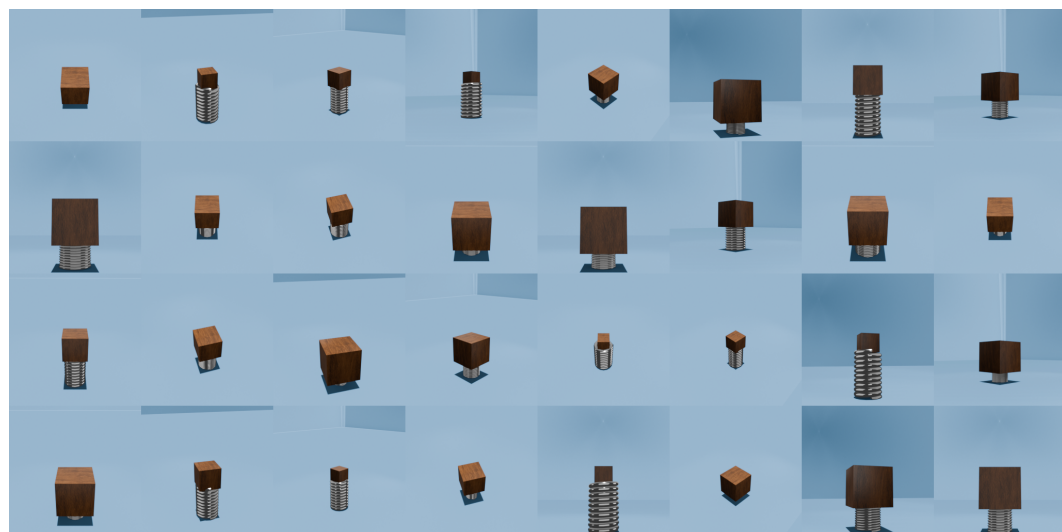


Figure 15: Spring (Virtual Background).

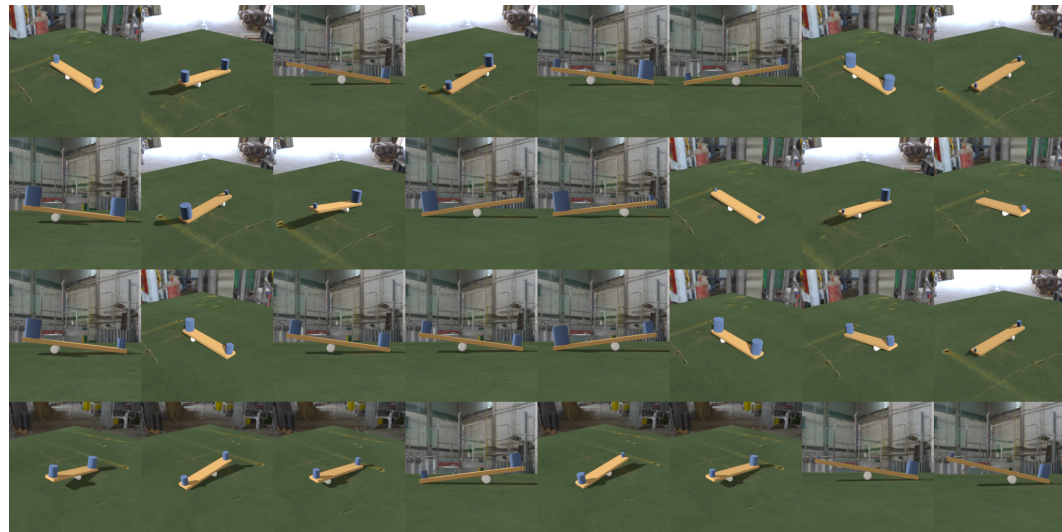


Figure 16: Seesaw (Real Background).

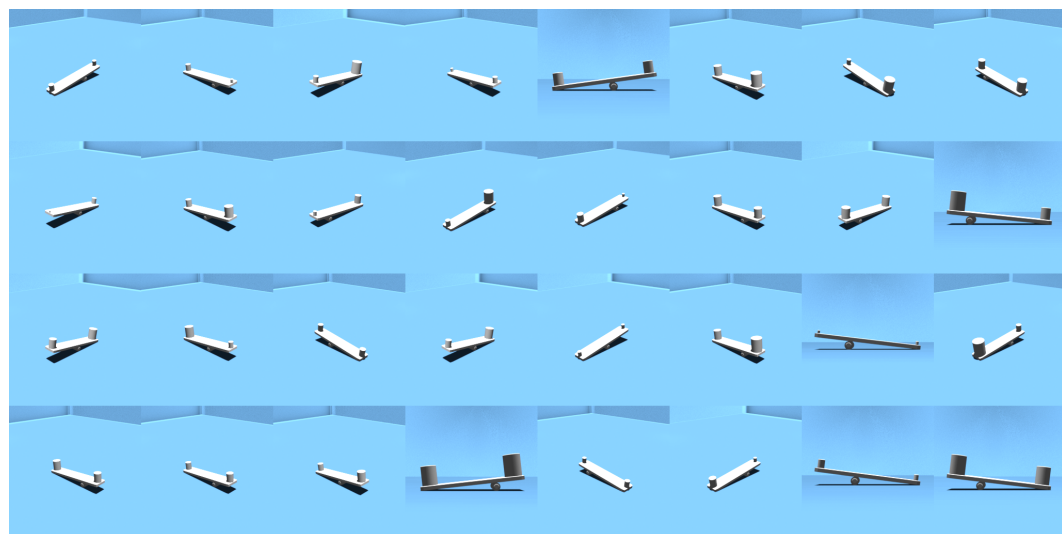


Figure 17: Seesaw (Virtual Background).

1026

1027

1028

1029

1030

1031

1032

1033

1034

1035

1036

1037

1038

1039

1040

1041

1042

1043

1044

1045

1046

1047

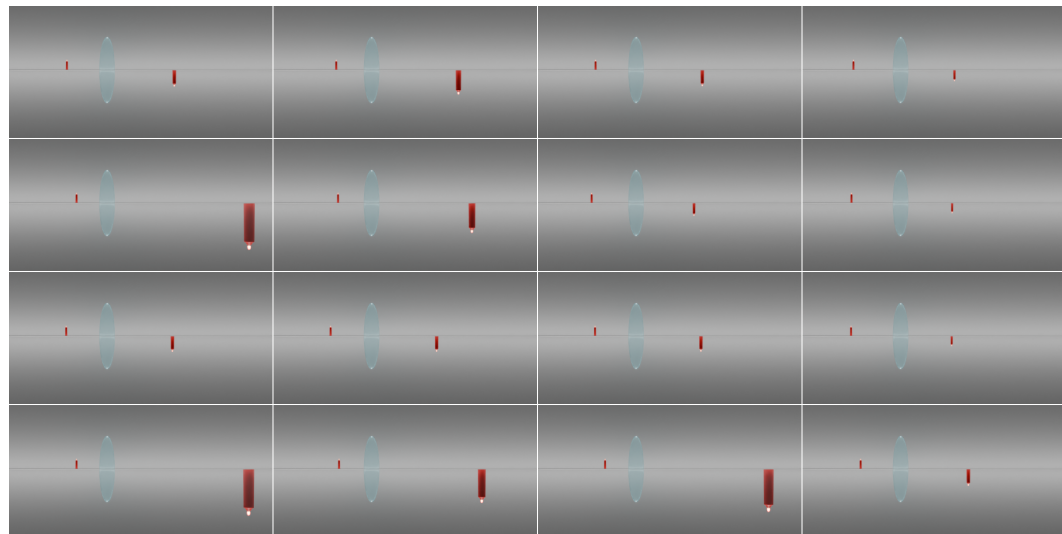


Figure 18: Convex Lens.

1048

1049

1050

1051

1052

1053

1054

1055

1056

1057

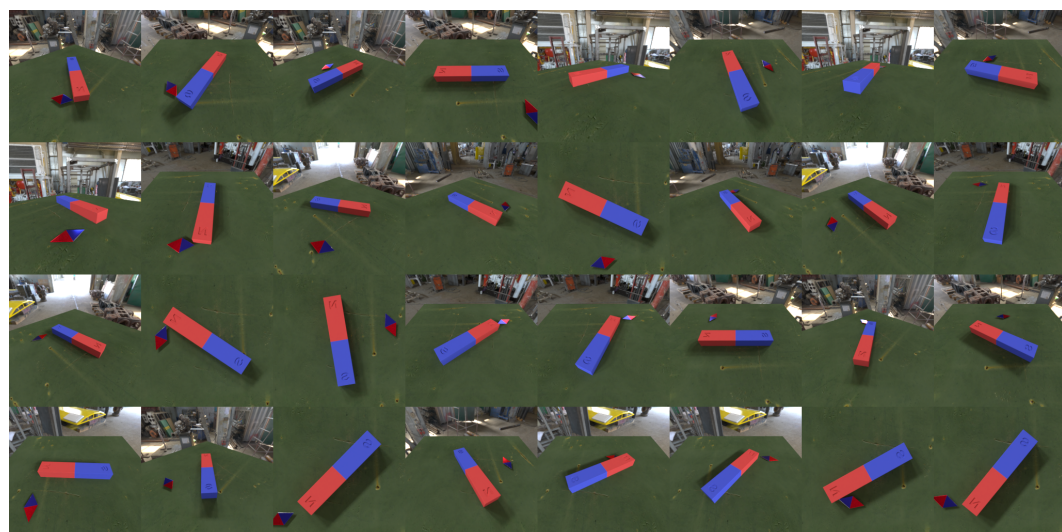


Figure 19: Magnet (Real Background).

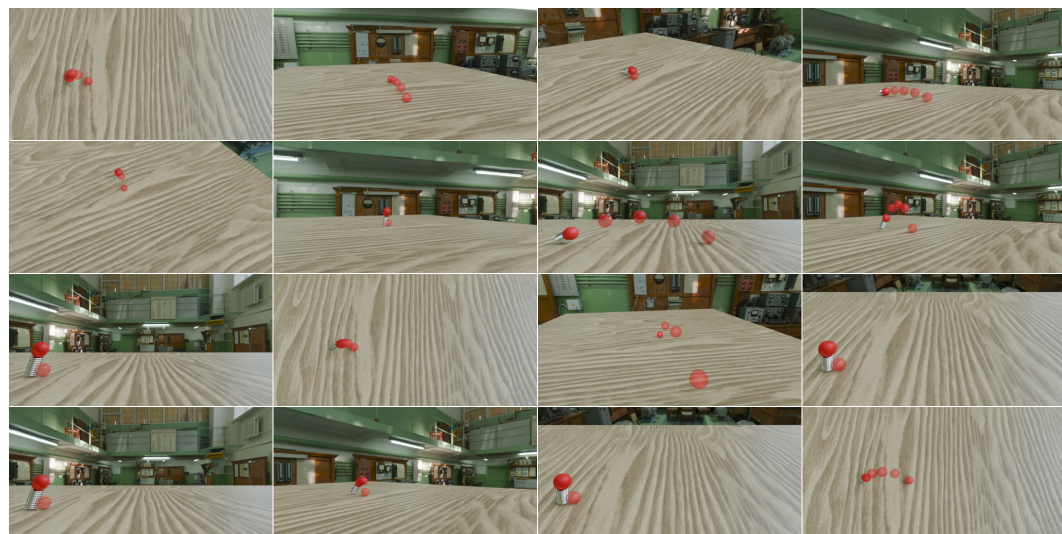
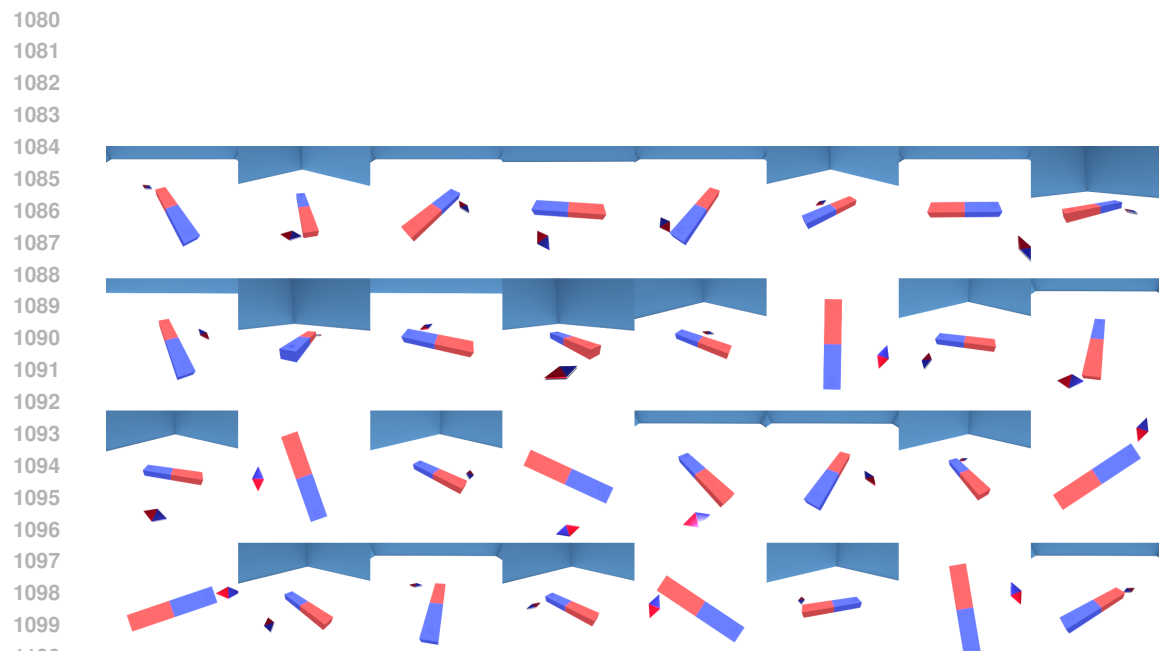
1075

1076

1077

1078

1079



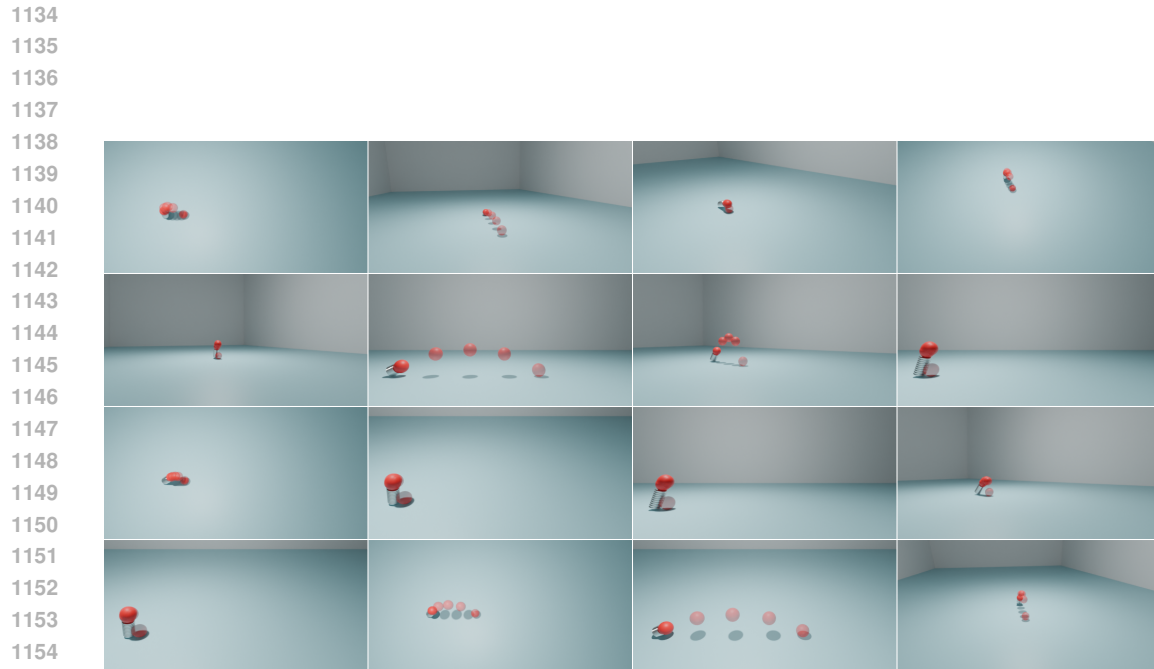


Figure 22: Parabola (Virtual Background).

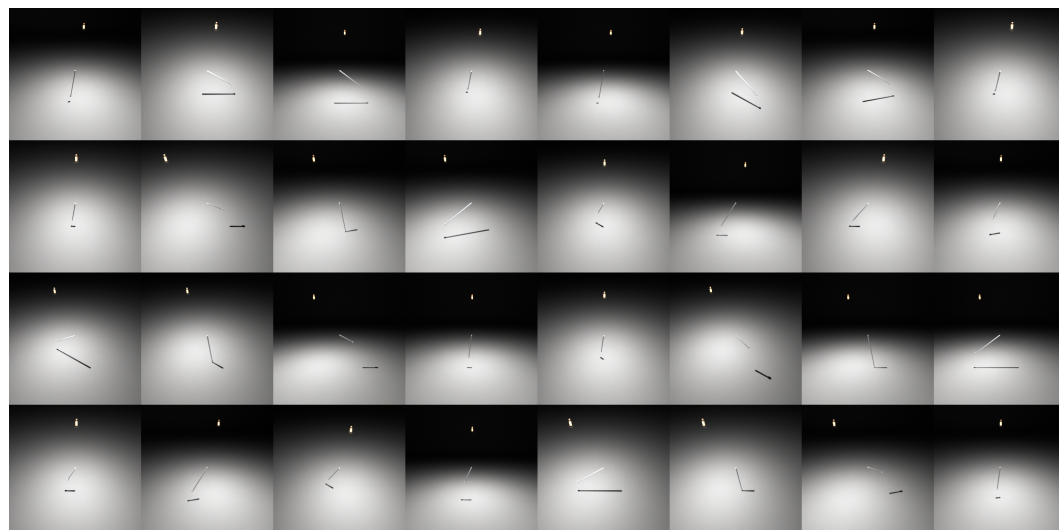


Figure 23: Pendulum.

1183
 1184
 1185
 1186
 1187

1188
1189
1190
1191
1192
1193
1194
1195
1196
1197
1198
1199
1200
1201
1202
1203
1204
1205
1206
1207
1208
1209

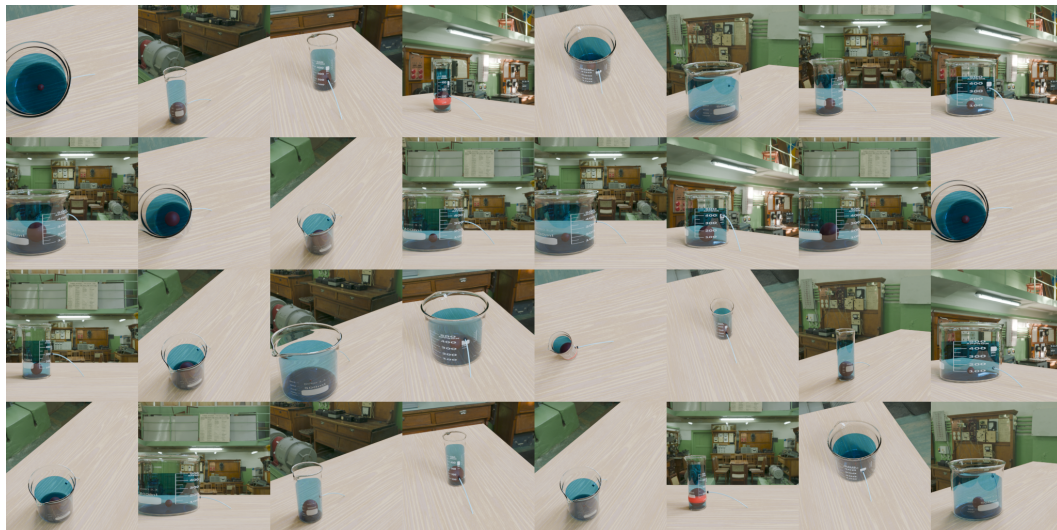


Figure 24: Water Flow (Real Background).

1210
1211
1212
1213
1214
1215
1216
1217
1218
1219



Figure 25: Water Flow (Virtual Background).

1237
1238
1239
1240
1241

1242
1243
1244
1245
1246
1247
1248
1249
1250
1251
1252
1253
1254
1255
1256
1257
1258
1259
1260
1261
1262

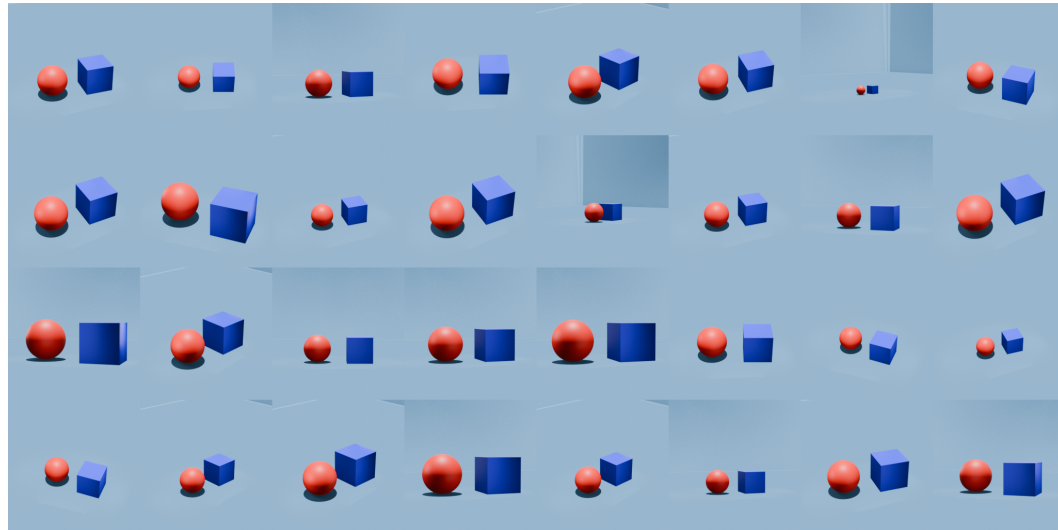


Figure 26: Hypothetical Scene (2 Variables, Linear).

1263
1264
1265
1266
1267
1268
1269
1270
1271
1272
1273
1274
1275
1276
1277
1278
1279
1280
1281
1282
1283
1284
1285
1286
1287
1288
1289
1290

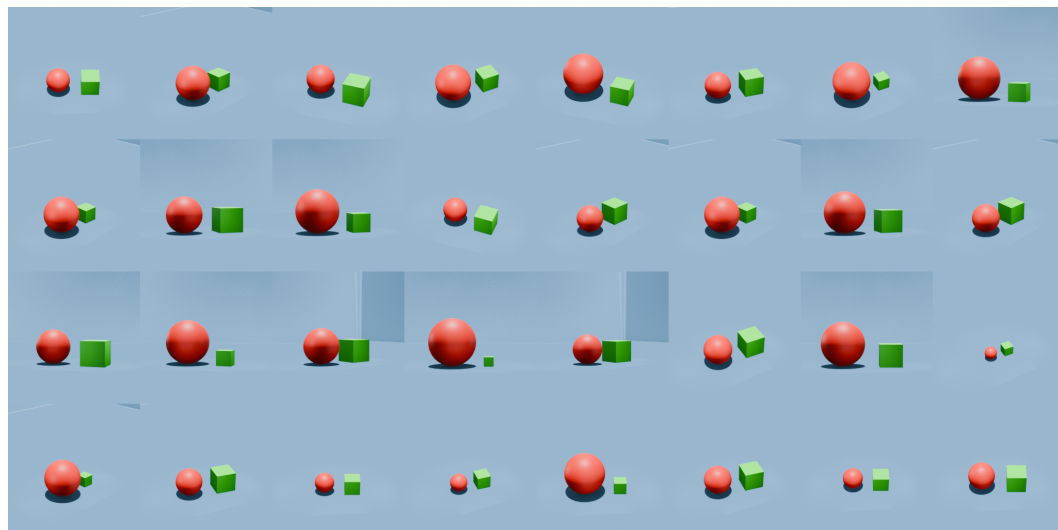


Figure 27: Hypothetical Scene (2 Variables, Non-Linear).

1291
1292
1293
1294
1295

1296
 1297
 1298
 1299
 1300
 1301
 1302
 1303
 1304
 1305
 1306
 1307
 1308
 1309
 1310
 1311
 1312
 1313
 1314
 1315
 1316
 1317

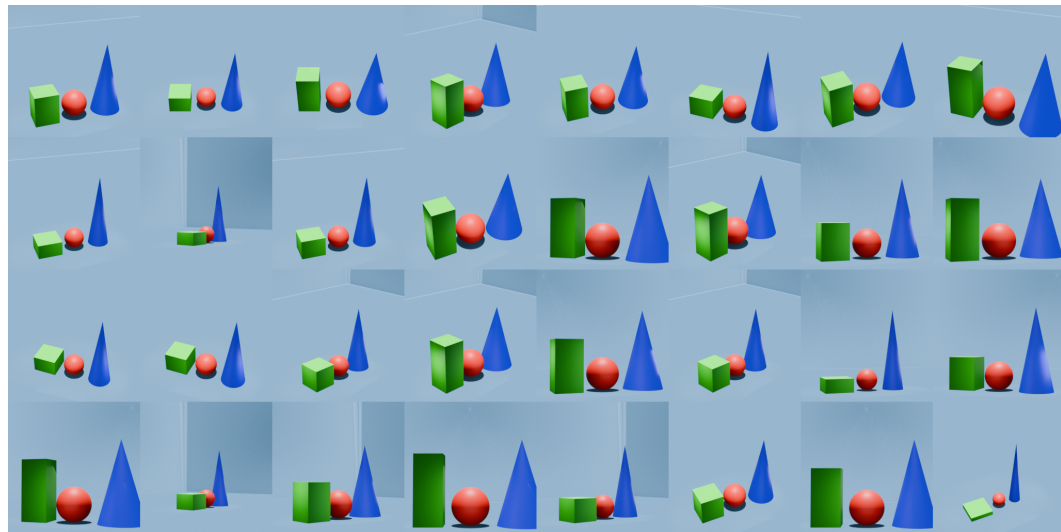


Figure 28: Hypothetical Scene (3 Variables, Linear, Fully-Connected).

1318
 1319
 1320
 1321
 1322
 1323
 1324
 1325
 1326
 1327
 1328
 1329
 1330
 1331
 1332
 1333
 1334
 1335
 1336
 1337
 1338
 1339
 1340
 1341
 1342
 1343
 1344

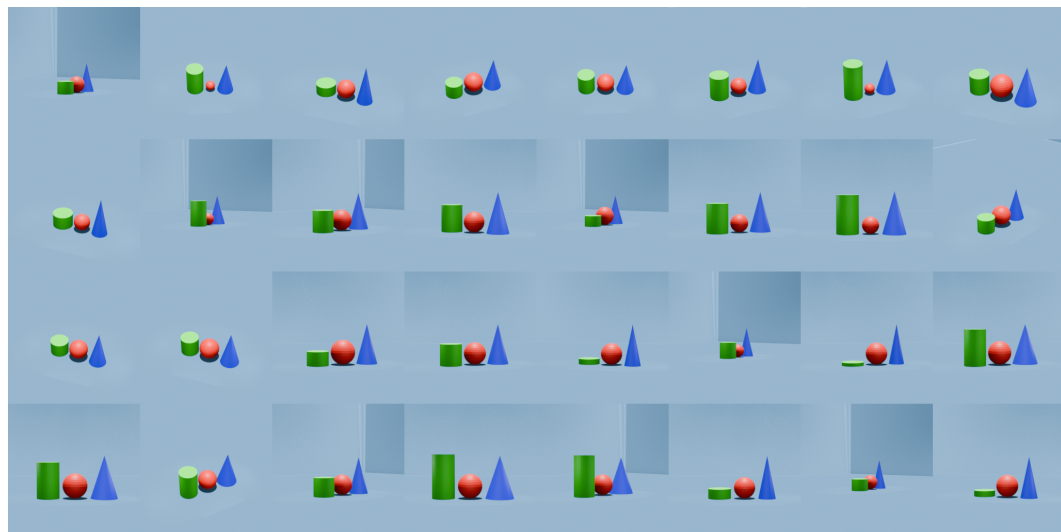


Figure 29: Hypothetical Scene (3 Variables, Linear, V-Structure).

1345
 1346
 1347
 1348
 1349

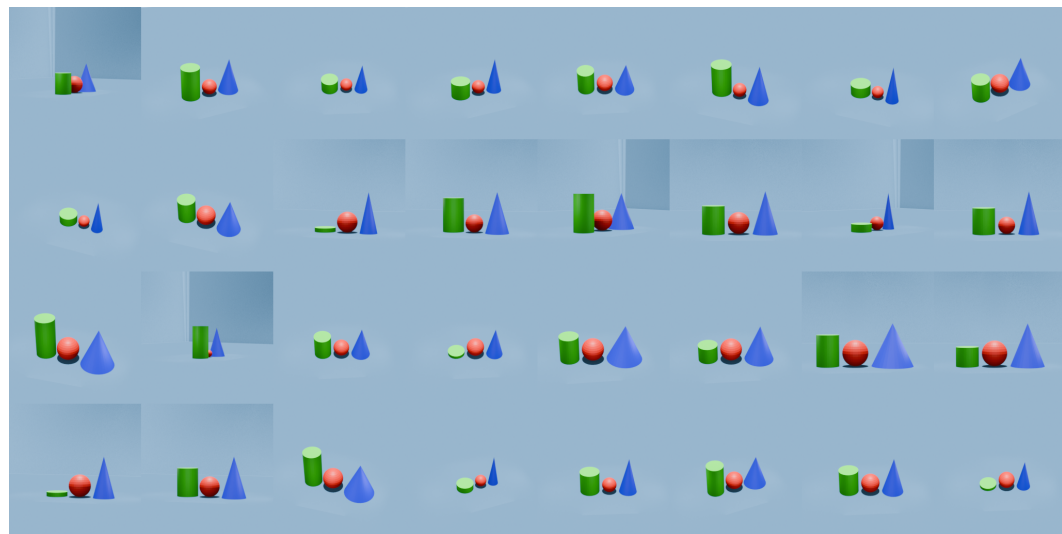


Figure 30: Hypothetical Scene (3 Variables, Non-Linear, V-Structure).

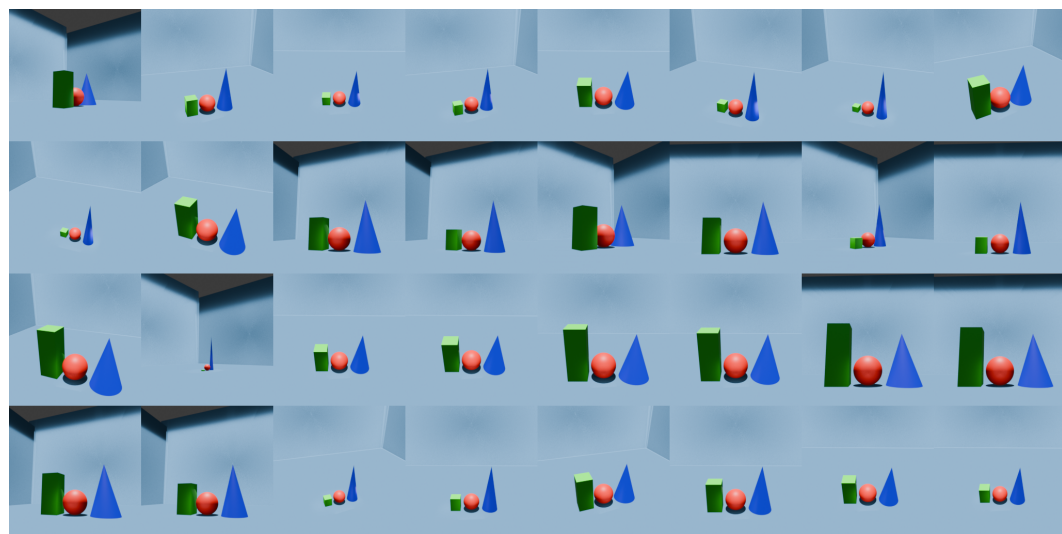


Figure 31: Hypothetical Scene (4 Variables, Linear, Fully-Connected).

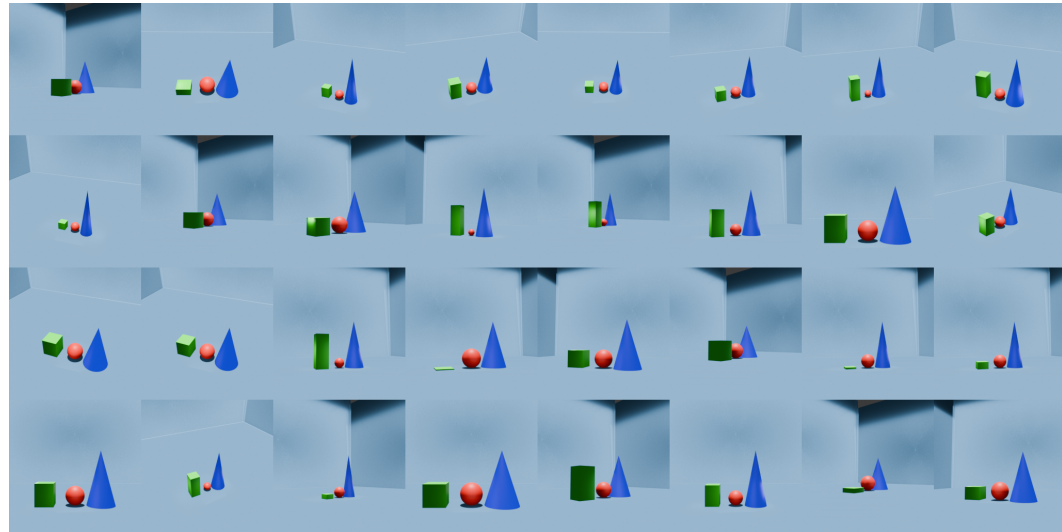


Figure 32: Hypothetical Scene (4 Variables, Linear, V-Structure).

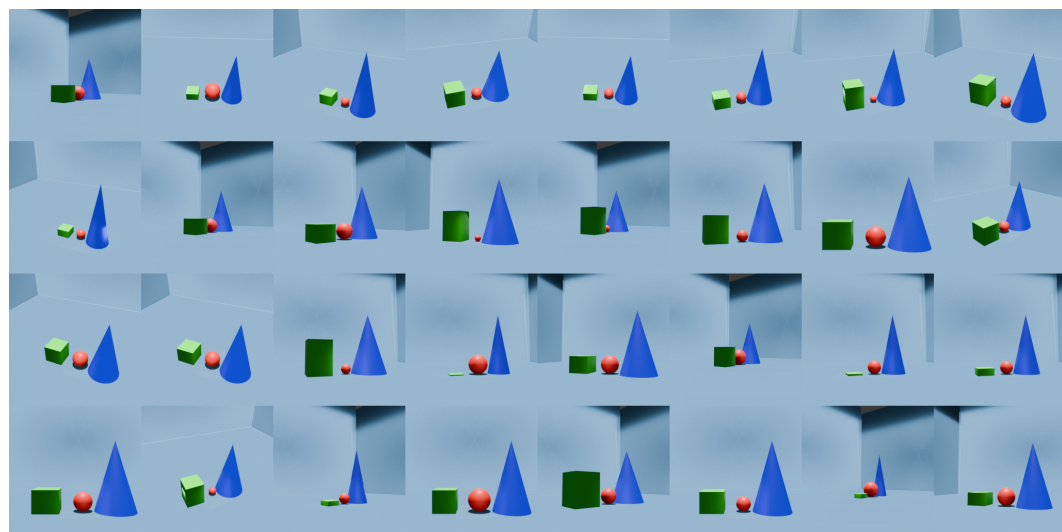


Figure 33: Hypothetical Scene (4 Variables, Non-Linear, V-Structure).

1458

1459

1460

1461

1462

1463

1464

1465

1466

1467

1468

1469

1470

1471

1472

1473

1474

1475

1476

1477

1478

1479

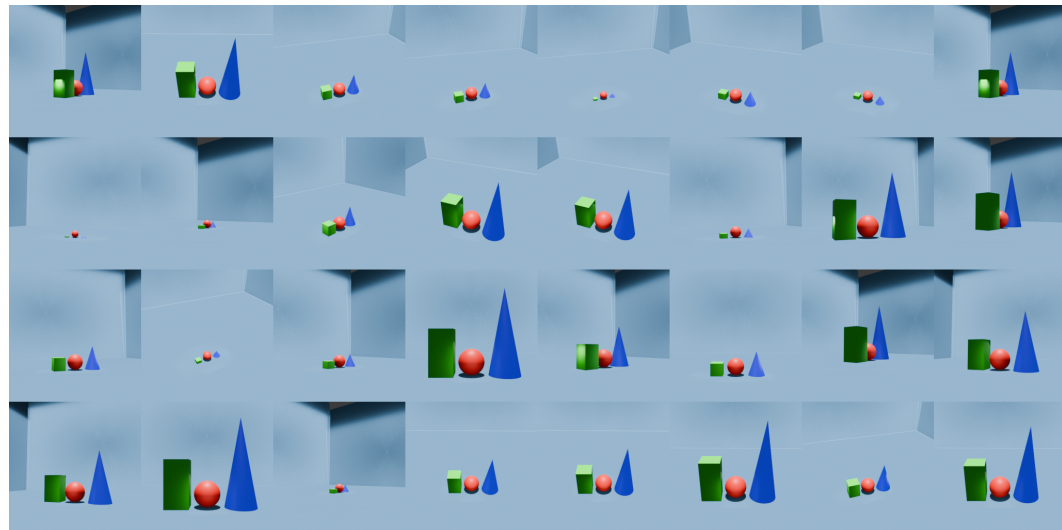


Figure 34: Hypothetical Scene (5 Variables, Linear, Fully-Connected).

1480

1481

1482

1483

1484

1485

1486

1487

1488

1489

1490

1491

1492

1493

1494

1495

1496

1497

1498

1499

1500

1501

1502

1503

1504

1505

1506

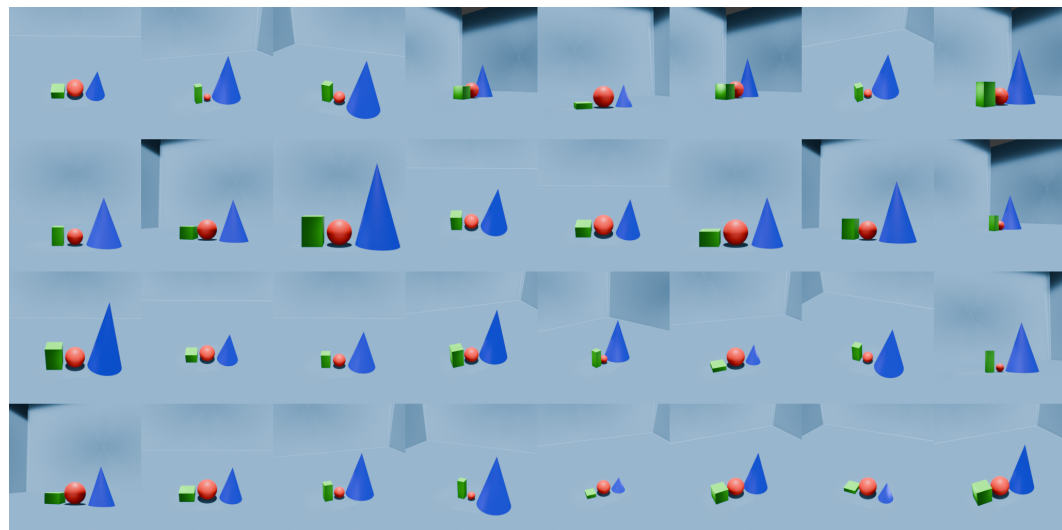


Figure 35: Hypothetical Scene (5 Variables, Linear, V-Structure).

1507

1508

1509

1510

1511

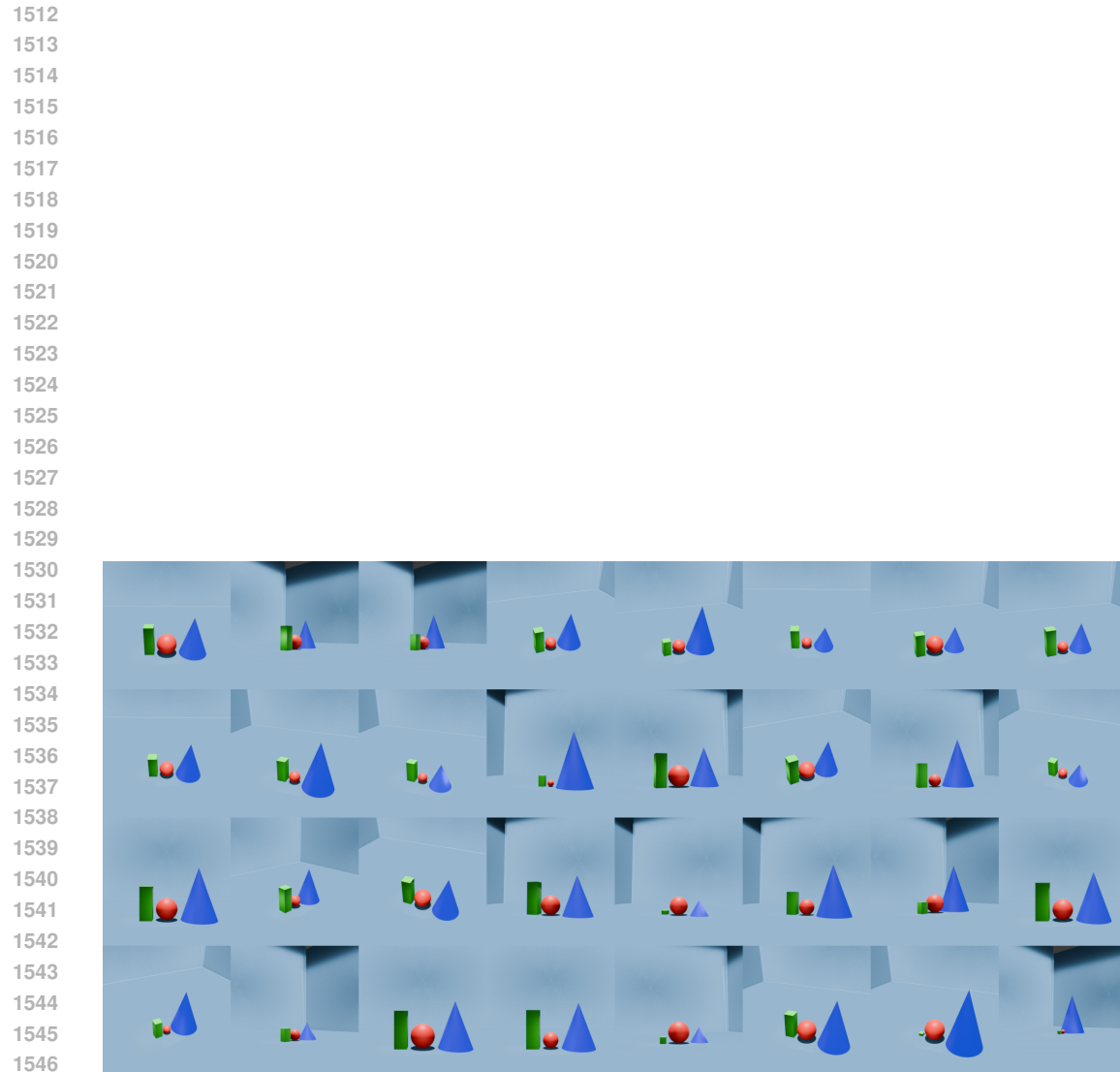


Figure 36: Hypothetical Scene (5 Variables, Non-Linear, V-Structure).

1566 7 EXPERIMENT DETAILS

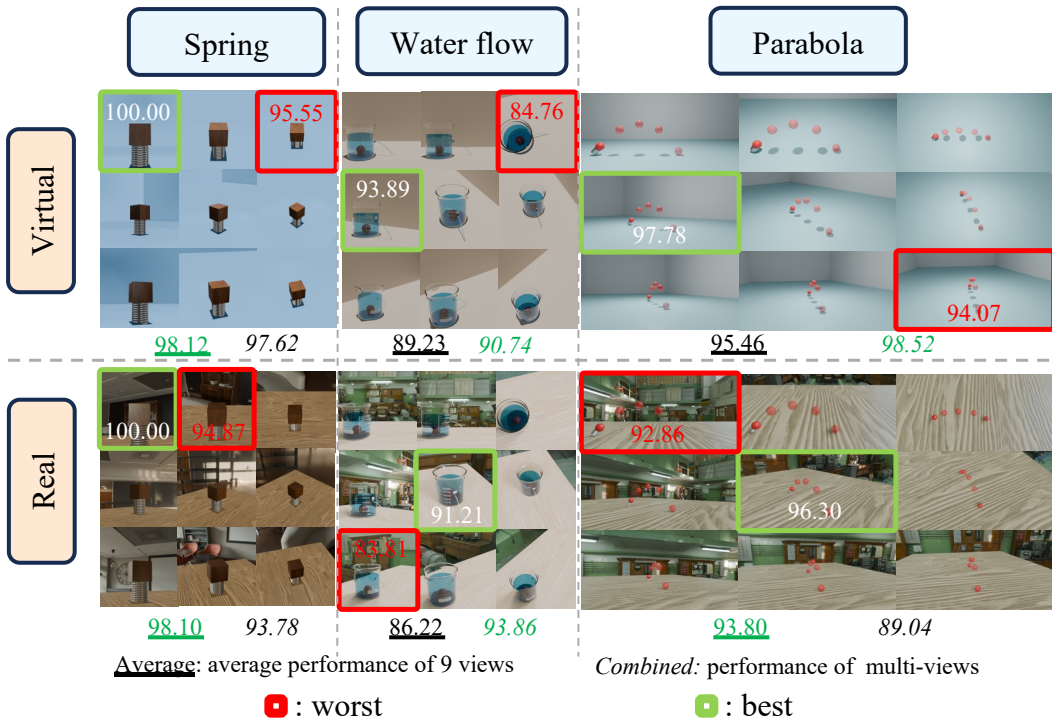
1568 In this section, we record the details in the experiments in the main paper.

1570 7.1 DIFFERENT PROMPTING STRATEGIES

1572 In the experiment of VLMs, we present four detailed prompt strategies for performing causal dis-
1573 covery tasks (see Tab. 5).

1575 7.2 EXPERIMENTAL RESULT OF THE IMPACT OF VIEWS AND BACKGROUNDS

1577 In the main paper, we evaluate the impact of different views and backgrounds on causal discovery
1578 with VLMs. As shown in Fig.37, we use multiple images with both realistic and virtual backgrounds
1579 in the experiments. Tab. 4 reports the concrete numerical results for each setting, which support our
1580 claims in Sec. 4.4.



1604 Figure 37: Performance Comparison in 3D scenes: selecting 3 scenes for case studies: Spring,
1605 Water flow, and Parabola. Using F1 score as the evaluation metric, we assess inference performance
1606 in the causal discovery task. The best and worst views are highlighted to demonstrate the impact
1607 of different perspectives. To analyze the effect of multi-view vs. single-view inputs, we average
1608 the performance across 9 individual views and compare it with the overall multi-view performance,
1609 highlighting the better results in green.

1612 8 BROADER IMPACT

1614 CAUSAL3D advances the integration of causal reasoning in computer vision, contributing to more
1615 robust, interpretable, and generalizable AI systems. By introducing a structured benchmark and
1616 systematically evaluating state-of-the-art methods, our research provides valuable insights into the
1617 challenges and opportunities of causal learning in visual data. The proposed benchmark fosters
1618 interdisciplinary collaboration, bridging causal inference, computer vision, and machine learning
1619 communities. It serves as a foundation for future research, enabling the development of models
that can better generalize across domains, adapt to distribution shifts, and provide meaningful

1620	100	100	95.56	86.87	90.07	84.76	94.09	94.42	95.56
1621	94.87	100	100	93.89	91.39	87.95	97.78	95.56	96.83
1622	97.62	97.78	97.22	88.79	91.10	88.22	95.11	95.70	94.07
1623									
1624	100	94.87	97.78	87.53	83.97	85.93	92.86	93.00	94.56
1625	100	97.44	97.62	81.71	91.21	83.82	93.11	96.30	94.04
1626	95.24	100	100	86.99	88.60	86.22	93.07	93.45	93.80
1627									

Table 4: Numerical results corresponding to Fig. 37. The table layout matches Fig. 37, and each value indicates performance under a specific view.

explanations. Furthermore, by improving causal understanding in vision tasks, this work has potential applications in fields such as healthcare, autonomous systems, and scientific discovery, where reliability and transparency are essential. While our evaluation framework is based on the authors' consensus, we encourage community discussions to refine causal reasoning criteria and enhance benchmarking standards. We will release evaluation scripts to support innovation and aid the development of new methodologies. Additionally, we emphasize the responsible use of CAUSAL3D and strictly prohibit any form of data leakage or test set optimization to maintain fairness and integrity in evaluation. Our work does not raise any ethical concerns that require disclosure.

9 LIMITATIONS

Although CAUSAL3D is comprehensive, there remains room for improvement. First, the current benchmark is constructed solely from observational data; incorporating interventional data in the future would enable user interaction and support more interactive causal evaluation. Second, the dataset complexity could be further enriched by introducing more nodes in the causal graphs and incorporating finer-grained visual details, such as textures of objects.

10 THE USE OF LARGE LANGUAGE MODELS (LLMs)

We used ChatGPT, Claude and Gemini to evaluate our datasets. The LLM was not involved in data generation, model training, or writing of technical content.

1674 Table 5: Examples of the four prompt strategies used for causal discovery tasks in VLMs evaluation.
1675

PROMPT STRATEGY	TEMPLATE EXAMPLE
BASIC	<p>ANALYZE THE PROVIDED IMAGES AND IDENTIFY CAUSAL RELATIONSHIPS BETWEEN THE VARIABLES. COMPLETE THE CAUSALITY ADJACENCY MATRIX BASED ON THE IDENTIFIED RELATIONSHIPS AND BRIEFLY EXPLAIN YOUR CONCLUSIONS. THERE ARE {VARIABLES}: X, Y, Z.</p> <p>PLEASE FILL THIS CAUSALITY ADJACENCY MATRIX:</p> $\begin{bmatrix} - & - & - \\ - & - & - \\ - & - & - \end{bmatrix}$ <p>IN THIS MATRIX, $\text{MATRIX}[i][j] = 1$ MEANS VARIABLE i CAUSES VARIABLE j, WHILE $\text{MATRIX}[i][j] = 0$ MEANS THERE IS NO DIRECT CAUSAL RELATIONSHIP.</p>
EXPLICIT FUNCTION	<p>YOU ARE A CAUSAL DISCOVERY EXPERT. YOUR OBJECTIVE IS TO ANALYZE THE PROVIDED IMAGES AND IDENTIFY ANY CAUSAL RELATIONSHIPS BETWEEN THE VARIABLES.</p> <p>USE THE IDENTIFIED RELATIONSHIPS TO COMPLETE THE CAUSALITY ADJACENCY MATRIX AND PROVIDE A BRIEF EXPLANATION SUPPORTING YOUR CONCLUSIONS. THERE ARE VARIABLES: X, Y, Z ...</p>
ZERO-SHOT-CoT	<p>ANALYZE THE PROVIDED IMAGES AND IDENTIFY CAUSAL RELATIONSHIPS BETWEEN THE VARIABLES ...</p> <p>LET'S THINK STEP BY STEP ...</p>
FEW-SHOT	<p>ANALYZE THE PROVIDED IMAGES AND IDENTIFY CAUSAL RELATIONSHIPS BETWEEN THE VARIABLES ...</p> <p>EXAMPLE 1: TO DETERMINE THE CAUSAL RELATIONSHIPS BETWEEN THE SPRING CONSTANT, WEIGHT, AND DEFORMATION OF THE SPRING, WE CAN USE HOOKE'S LAW, WHICH STATES THAT THE FORCE EXERTED BY A SPRING IS DIRECTLY PROPORTIONAL TO THE DEFORMATION (DISPLACEMENT) OF THE SPRING, GIVEN BY:</p> $F = k \cdot x$ <p>WHERE:</p> <ul style="list-style-type: none"> • F IS THE FORCE APPLIED (RELATED TO WEIGHT), • k IS THE SPRING CONSTANT, • x IS THE DEFORMATION OF THE SPRING. <p>FROM THIS, WE CAN INFER:</p> <ol style="list-style-type: none"> 1. SPRING CONSTANT k AFFECTS THE DEFORMATION OF THE SPRING (x): IF THE SPRING CONSTANT INCREASES, FOR THE SAME WEIGHT, THE DEFORMATION DECREASES. 2. WEIGHT AFFECTS DEFORMATION OF THE SPRING (x): AN INCREASE IN WEIGHT CAUSES MORE DEFORMATION. 3. THE SPRING CONSTANT (k) AND WEIGHT DO NOT DIRECTLY AFFECT EACH OTHER. <p>BASED ON THESE RELATIONSHIPS, THE CAUSALITY ADJACENCY MATRIX IS:</p> $\begin{bmatrix} 0 & 0 & 1 \\ 0 & 0 & 1 \\ 0 & 0 & 0 \end{bmatrix}$ <p>EXPLANATION:</p> <ul style="list-style-type: none"> • ELEMENT (1,3) IS 1 BECAUSE THE SPRING CONSTANT AFFECTS DEFORMATION. • ELEMENT (2,3) IS 1 BECAUSE THE WEIGHT AFFECTS DEFORMATION. • THE OTHER ENTRIES ARE 0 BECAUSE THERE IS NO DIRECT CAUSAL RELATIONSHIP OTHERWISE. <p>EXAMPLE 2: ...;</p> <p>EXAMPLE 3: ... ;</p>